Realia et naturalia

DISSERTATIONES
CHIMICAE
UNIVERSITATIS
TARTUENSIS
135

JÜRI LIIV

PVDF (polyvinylidene difluoride) as material for active element of twisting-ball displays

TARTU ÜLIKOOL · UNIVERSITAS TARTUENSIS · 1632

DISSERTATIONES CHIMICAE UNIVERSITATIS TARTUENSIS
135

DISSERTATIONES CHIMICAE UNIVERSITATIS TARTUENSIS
135

JÜRI LIIV

PVDF (polyvinylidene difluoride) as material for active element of twisting-ball displays

UNIVERSITY OF TARTU
PRESS
1632

Institute of Chemistry, Faculty of Science and Technology, University of Tartu, Estonia

Dissertation is accepted for the commencement of the degree of Doctor of Philosophy in Chemistry on April 29th, 2014 by the Council of Institute of Chemistry, University of Tartu.

Supervisors: Professor Jaak Järv (PhD, DrChem), Professor Toomas Tenno (PhD)

Opponent: Professor Senentxu Lanceros-Méndez (PhD), Universidade do Minho, Portugal

Commencement: June 17th, 2014, at 10:00. Ravila 14a, 1021, Tartu

Publication of this dissertation is granted by University of Tartu, Estonia.

ISSN 1406–0299
ISBN 978–9949–32–566–5 (print)
ISBN 978–9949–32–567–2 (pdf)

University of Tartu Press
www.tyk.ee

CONTENTS

1. LIST OF ORIGINAL PUBLICATIONS

I **Liiv, J**., Zekker, I., Panov, D., Sammelselg, V., Tenno, T., Järv, J. Chemical functionalization of a polyvinylidene fluoride surface. Polym. J. 45, 313–317 (2012).doi:10.1038/pj.2012.148

II **Liiv, J.**, Panov, D., Tenno, T., Järv, J. Alumina coating of polyvinylidene fluoride (PVDF) surface in liquid phase. Surf. Eng. 30(4), 268–271 (2014). doi:10.1179/1743294414Y.0000000246

III **Liiv, J.**, Maširin, A., Tenno, T, Miidla, P. Mathematical modeling of performance of the twisting-ball display. P. Est. Acad. Sci. 63 (2014). [In press]

IV **Liiv, J.**, Tenno, T., Järv, J. Polarization of polyvinylidene difluoride particles for use as active elements of a twisting-ball display. Funct. Mat. Lett. [Forthcoming]

V **Liiv, J.** Active optical element, method of producing the same. Estonian patent EE 05070, US patent US 08383010

VI Miidla, P., **Liiv, J.**, Maširin, A., Tenno, T. Simulation of a twisting-ball display cell. Mathematics in Industry. Proceedings of the 18th European Conference on Mathematics for Industry. Bock, H.G. et al, Eds. Springer (2014). [In press]

Author's contribution:

Paper I: Responsible for planning and performing the experiments. Responsible for preparing the manuscript.

Paper II: Responsible for planning and performing the experiments. Responsible for preparing the manuscript.

Paper III: Participated in mathematical modeling. Responsible for writing the manuscript.

Paper IV: **R**esponsible for planning and performing the experiments. Responsible for writing the manuscript.

Paper V: Inventor.

Paper VI: Participated in mathematical modeling and in manuscript preparation.

2. ABBREVIATIONS AND SYMBOLS

ACS	American Chemical Society
ATR FT-IR	attenuated total reflection Fourier transform infrared spectroscopy
ATRP	atom transfer radical polymerization
bp	boiling point
bpy	2,2'-bipyridine
CAS	Chemical Abstracts Service registry number
DSC	differential scanning calorimetry
F_E	electrostatic force
F_L	viscous drag
FIB	focused ion beam introduction
FT-IR	Fourier transform infrared spectroscopy
ITO	indium tin oxide
J	moment of inertia of the ball
m	mass of the particle
M_E	electrostatic torque
M_J	inertial torque
M_S	viscous torque
Me4CYCLAM	1,4,8,11-tetraaza-1,4,8,11-tetramethylcyclotetradecane
Me6TREN	tris[2-(dimethylamino)ethyl]amine
Mw	molar weight
n	coefficient of expansion of the elastomer sheet
PDMAEMA	poly[2-(N,N-dimethyl amino)ethyl methacrylate]
PPEGMA	poly[poly(ethylene glycol) monomethacrylate]
PVDF	polyvinylidene fluoride
r	radius of the ball
r_c	radius of the cavity
r_D	radius of the dipole
R_D	thickness of the silicone film
q	monopolar charge of the particle
q_D	dipole charge
s	thickness of the elastomer sheet
SEM	scanning electron microscope
TMEDA	N,N,N',N'-tetramethylethylenediamine
tpy	2,2':6',2''-terpyridine
TREN	tris(2-aminoethyl)amine
U_c	control voltage
y	shift
ρ	density of PVDF
$\acute{\eta}$	viscosity of the fluid

3. INTRODUCTION

A twisting-ball display[1] is a kind of electrophoretic information display invented at the Xerox Palo Alto Research Center (PARC) and called “Gyricon” (Fig. 1). This kind of display consists of a thin layer of transparent silicone where bichromal spherical polarized particles (“balls”) are dispersed. In the Xerox Gyricon project these balls, forming the active display elements, were made of different waxes and were charged by a stochastic process that caused each particle to have different and relatively low charge. Therefore, the required control voltages were high[2] and the quality of the produced image was insufficient for market needs. In the 1990s Xerox discontinued Gyricon R&D activities.

The author of this work suggested an alternative method[3] for preparing the bichromal polarized particles, made of polyvinylidene difluoride (PVDF). This material is an electret with an extremely high residual electric field[4]. During the polarization process the –CF groups align themselves in the crystal structure of the dielectric material following the direction of the electrostatic field, producing a permanent electrostatic bias. Therefore, it was suggested that the electret properties of this material could be used for preparation of the active elements for the twisting ball display.

However, as PVDF is chemically inert material, its usage in this kind of applications wasn't possible until efficient process of chemical modification of its surface with polystyrene layer[5] and thereafter coating with a non-transparent alumina layer[6] was proposed (Papers I and II). As a relatively thick layer of inorganic material was needed for the “twisting ball” display elements, a new approach for directed alumina deposition was invented, starting from alumina formation from interior of the polystyrene layer. Afterwards the alumina-covered particles were polarized, colored and deposited into transparent silicone film placed between two control electrodes (Paper IV). One of these electrodes was transparent glass plate covered with ITO (indium tin oxide). The behavior of the particles in this model display element was compared with the theoretical model[7] also proposed in this dissertation (Papers IV and VI).

4. LITERATURE OVERVIEW

4.1. Twisting-ball display – state of the art

E-paper (reflective) displays are fundamentally different from the conventional emissive flat panel displays as backlight liquid crystal displays (LCD), plasma display panels (PDP) and light emitting diode (LED) displays in the following way: they reflect ambient light lake paper and are extremely energy efficient. This increases battery lifetime in portable devices, as their power consumption, when displaying a static image, is zero. They only require power when changing the image or presenting video (bi-stability). Therefore, these devices could be low cost, robust, durable and flexible, and can be (eventually) made on plastics using roll-to-roll manufacturing methods.

One possibility to meet these basic requirements is to apply the "twist ball technology"[8], where the display image is created in a thin transparent layer containing bichromal spherical particles that are polarized towards the differently colored hemispheres (Fig. 1). This kind of display was invented by the Xerox Palo Alto Research Center (PARC) and these principles were used in several products. Each ball is an electrical dipole and should be placed in the cavity in the transparent silicone film filled with dielectric fluid. The diameter of the cavity is 10–30% greater than the diameter of the balls. When the control voltage is constant or zero, the ball should be fixed.

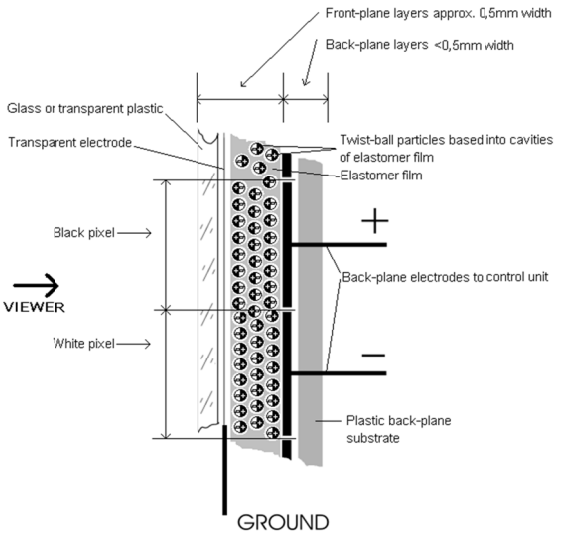

Figure 1. Model of the "twisting ball" display. Cross-section of the twisting-ball display is shown, where we can see poled and colored particles in the silicone film between the control electrodes.

When the polarity of the control voltage is changed, the ball begins to move towards the opposite wall of the cavity[9]. Microscopic asymmetries and the "rolling effect" cause a deviation of the axis of the electrical dipole from the direction of the electrical field. Then an electrostatic torque appears and causes the ball to rotate and different colored hemisphere will be exposed to the viewer. The displays based on such physical principles are highly bi-stable, robust, easy to manufacture and have very low power consumption as the image is being formed using ambient light, similar to conventional printed paper.

The active elements (balls) of Xerox Gyricon displays were made of different waxes or polyethylene[2] and were charged by a stochastic process that caused each particle to have a slightly different charge. Because of this the dipole charges of the balls were low and unequal and the required control voltages were high. Therefore, the quality of the image was insufficient for market needs. It was suggested that preparation of more uniformly polarized particles may be needed to improve the quality of the image and therefore PVDF as an electrets material was selected for this work.

4.2. Methods for PVDF surface modification

Physical properties of PVDF can be modified using a controlled length of PVDF chain[10], copolymerization of PVDF with another monomers[11] or compounding of PVDF with inorganic nanomaterials. Unfortunately these methods do not allow for modifying the surface of a polymer that remains chemically inert and hydrophobic.

Most of the known chemical methods of surface grafting have not been effective with PVDF and therefore some more reactive polymers, like cyanoacrylate, have been blended into the fluoropolymer to increase reactivity and hydrophilic properties of the material[12]. However, this blending has always worsened quality of the material, especially if the electric properties of this polymer are considered. Therefore, we were focusing on the grafting of pure PVDF surface and analyzed the methods which could be useful for its functionalization.

In some studies treatment of PVDF by high energy beams or plasma was used[13]. After the plasma treatment the hydrophilic properties of PVDF significantly increased, resulting, for example, in a decrease of the PVDF/H_2O contact angle from 90° to 70°. Different fluoropolymers were also functionalized by various oxygen-containing functional groups by treatment with a concentrated aqueous solution of lithium hydroxide[14] or ammonia solution of lithium[15] or magnesium amalgam[16]. However, in all these cases sufficient surface activation has not been achieved without significant damage of the polymer interior structure and its contamination with the degradation products.

4.3. Atom transfer radical polymerization (ATRP)

Atom transfer radical polymerization[17] (ATRP) is a living polymerization via forming a carbon-carbon bond through a transition metal catalyst. ATRP is based on an inner sphere electron transfer process, which involves a reversible homolytic (pseudo)halogen transfer between a dormant species, an added initiator or dormant propagating chain end (R-X or R-P_n-X) and a transition metal complex in the lower oxidation state (Mt^m/L_n) (M^{tm} represents the transition metal species in oxidation state m and L is a ligand), resulting in the formation of propagating radicals ($R^{\bullet}$) and the metal complex in the higher oxidation state with a coordinated halide ligand (e.g. X-Mt^{m+1}/L_n). (Fig. 2).

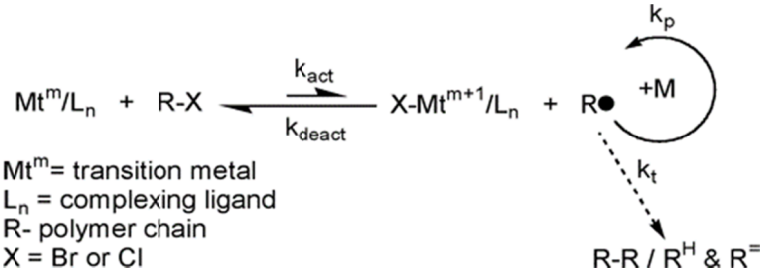

Figure 2. Chemistry of ATRP reaction.

The schematic presentation of the ATRP equilibria is shown in Fig. 3, which emphasizes the repetitive nature of the activation and deactivation steps and the need to push the equilibrium to the left, thereby forming a low concentration of radicals to reduce radical-radical termination reactions, and ensure a high mole fraction of dormant chains[17]. ATRP requires reactivation of the first formed alkyl halide adduct with the unsaturated compound (monomer) and the further reaction of the intermittently formed radical with additional monomer units (propagation).

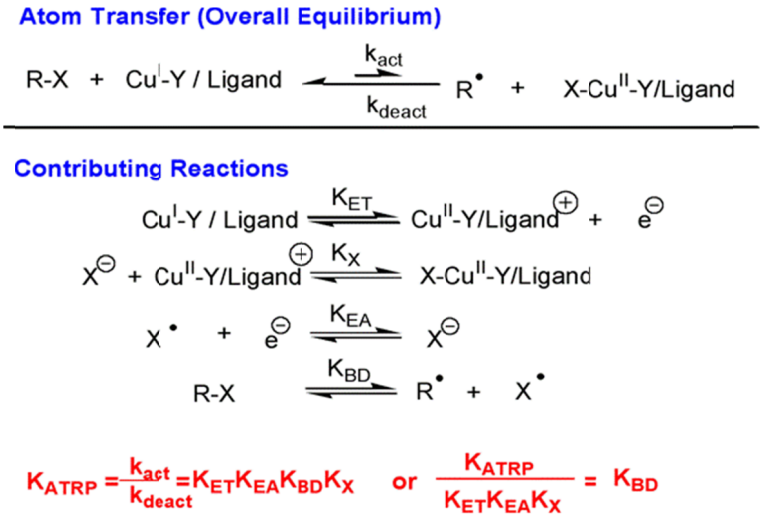

Figure 3. Equilibria, involved in the ATRP reaction.

The conventional version of the ATRP method requires the presence of an initiator and catalyst, and in this process radicals are generated through one electron oxidation of the initiator in a reversible redox process catalyzed by a transition metal-amine complex. Different amines have been used in this complex: 2,2'-bipyridine (bpy), N,N,N',N'-tetramethylethylenediamine (TMEDA), 2,2':6',2"-terpyridine (tpy), tris[2-(dimethyl amino)ethyl]amine (Me6TREN), 1,4,8,11-tetraaza-1,4,8,11-tetramethylcyclotetradecane (Me4CYCLAM), tris[2-aminoethyl]amine (TREN), etc.

Different transferable atoms or groups can participate in an ATRP, but the most frequently employed radically transferable atoms are halogens and will be used to exemplify ATRP throughout the following discussion. The ATRP equilibrium, (K_{ATRP} in the scheme above), is expressed as a combination of several contributing reversible reactions, including a combination of C-X bond homolyzis of the alkyl halide (R-X), two redox processes, and heterolytic cleavage of the CuII-X bond. Therefore, K_{ATRP} can be expressed as the product of the equilibrium constants for electron transfer between metal complexes (K_{ET}), electron affinity of the halogen (K_{EA}), bond dissociation energy of the alkyl halide (K_{BD}) and the equilibrium constant for the heterolytic cleavage of the Mt^{n+1}-X bond (K_X), which measures the "halidophilicity" of the deactivator. This means that for a given alkyl halide, R-X, the activity of a catalyst in an ATRP reaction not only depends on the redox potential, but also on the halidophilicity of the transition metal complex. For complexes that have similar halidophilicity, the redox potential can be used as a measure of catalyst activity in the ATRP.

Alkyl halides RX are typically used as initiators and the halide group must rapidly and selectively migrate between the growing chain and the transition-metal complex. If bromine and chlorine are good leaving groups, the energy of

the homolytic cleavage of the C-F bond is much higher and therefore fluorine has generally been considered a bad leaving group in ATRP[18].

This was probably the reason why practically no data about C-F bond participation in polymerization reactions of this type could be found, except the study of Chen et al[19] where direct atom transfer radical polymerization (ATRP) of poly[2-(N,N-dimethyl amino)ethyl methacrylate] (PDMAEMA) and poly[poly(ethylene glycol) monomethacrylate] (PPEGMA) on the surface of PVDF films was studied for biomedical purposes. PDMAEMA and PPEGMA were grafted to PVDF apparently by the ATRP mechanism with polymer initiation at the secondary fluorinated site.

Following this study, we developed a chemical method for modification of PVDF surface by polystyrene "brushes", which grow from the fluoropolymer surface where mono-functional initiator sites were activated. In the absence of thermal self-initiation and chain transfer phenomena this "grafting from" process was easy to control and yielded uniform and a high quality polystyrene layer.

4.4. Alumina precipitation from solutions

The various chemical reactions for the formation of nonstoichiometric boehmite ($Al_2O_3 \times xH_2O$, $1<x<1,5$) can be presented by the following reaction schemes [20]:

$$Al_2(SO_4)_3 + 3NH_2\text{-}CO\text{-}NH_2 + (x+6)H_2O \rightarrow Al_2O_3 \times xH_2O + 3(NH_4)_2SO_4 + 3CO_2$$

$$Al_2(SO_4)_3 + NH_2\text{-}CO\text{-}NH_2 + (x+7)\ H_2O \rightarrow Al_2O_3 \times xH_2O + 3(NH_4)_2SO_4 + 2NH_3 + 4CO_2$$

$$Al_2(SO_4)_3 + 7NH_2\text{-}CO\text{-}NH_2 + (x+14)\ H_2O \rightarrow Al_2O_3 \times xH_2O + 3(NH_4)_2SO_4 + 4(NH_4)_2CO_3 + 3CO_2$$

For precipitation of hydroxides and hydrous oxides in the water solution to insure the homogeneity of the deposition[21], the necessity for a careful control of pH in all volume of the reaction mixture is obvious. The best method of accomplishing this result[22] will be the use of a substance that slowly decomposes and neutralizes the acid. The following types of reagents have been used in an attempt to maintain the proper pH: buffers, such as acetic acid and acetate; insoluble oxides and carbonates, such as zinc oxide; weak bases, mostly organic, such as phenylhydrazine and pyridine; compounds which decompose with liberation of ammonia, such as hexamethylenetetramine and potassium cyanate; substances that decompose in hot solution with the formation of a volatile acidic constituent, such as sodium thiosulfate and ammonium nitrite; mixtures of halides, halates and halogen acids, such as iodate and iodide, bromate and bromide, bromate and chloride.

Using urea allows relatively easy control of the reaction conditions. Since this compound is well soluble in water and the rate of its decomposition into ammonia and carbon dioxide is dependent upon temperature, it was suggested to use this option for control of the pH of the reaction mixture, as the increase in pH can be stopped at any time by cooling. The pH of the solution cannot rise very high and the more alumina will not be precipitated, since the ammonia produced evaporates from the hot solution if the pH is above 7. The slow formation of carbon dioxide, produced by the decomposition of the urea, effectively prevents humping. In such a solution the change of pH will be uniform throughout, insofar as the temperature is the same, and no local excess of the reagent will be present in any point. Consequently, the hydroxide should be precipitated slowly and uniformly throughout the solution. This method fulfils simultaneously the requirements of homogeneity of solution, slow precipitation and easy control of the final pH in an entirely satisfactory manner. Such formation of monodispersed alumina particles from aluminium salt – urea solution was described by Sugimoto[21], who succeeded to avoid conglomeration of the particles by proper selection of the precipitation speed.

4.5. Poling of PVDF

Electret is a dielectric material exhibiting a quasi-permanent electrical charge[23]. There exist two different types of electrets: the first type with monopolar charge and the second with dipolar charge ("real" electrets). The former type includes materials where the excess charges are trapped for long time after charging (with electron or ion beam, etc.). In the latter type dipolar molecules or parts of crystal structure are oriented after the poling process (high electrical field, stretching, etc.). The average charge of the electrets remains unchanged but the sides of the material will have electrostatic charges of different polarity. Therefore, electret is an electrostatic analogue of a permanent magnet.

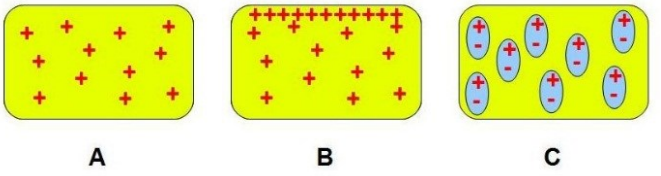

Figure 4. Schematic cross-section of different types of polarized electrets. A represents an electret with monopolar space charges; B with monopolar space charges and surface-charge layer and C with dipolar charges.

Fig. 4 shows the schematic cross-sections of different types of electrets. Here we see that charged electrets of the first type (A and B) have an excess charge,

trapped in the volume of the material. The overall charge of the electrets of the second type ("true" electrets) has a volume charge equal to zero. If the materials of this type are not poled, the orientation of dipoles is random (see Fig. 5). In many materials the electric fields may be compensated within a short time period by the motion of charges and dipoles. Materials with dipolar charges show higher electrical field and time stability than materials with introduced charges. Therefore, they are suitable for using as materials for twisting-ball displays.

Polyvinylidene difluoride (PVDF) has been proposed as an ideal candidate for electret applications as it exhibits a remnant polarization[23]. The enhanced thermal stability of the polarization is directly related to the high Curie' temperature, whereas the ferroelectric properties are related to the molecular packing as derived from the refined crystal structure.

PVDF, which has the following chemical structure, $(–CH_2\text{-}CF_2–)n$, is a semi-crystalline polymer with at least four different polymorphs referred to as the α, β, γ and δ phases, previously called in order of their discovery form II, I, III and IV, respectively[24]. Their crystal structures and phase transitions were thoroughly investigated in the 1970s and 1980s. Thermodynamically, the most stable phase at ambient temperature and pressure is the α phase. Owing to the centro-symmetric symmetry of the unit cell, the α phase is non-polar and paraelectric. β phase PVDF is thermodynamically more stable than α-PVDF. The unit cell of β-PVDF has a macroscopic dipole moment rendering it ferroelectric. Thick paraelectric α-PVDF can be converted into free-standing ferroelectric β-PVDF films by biaxial stretching or high electric field (Fig. 5).

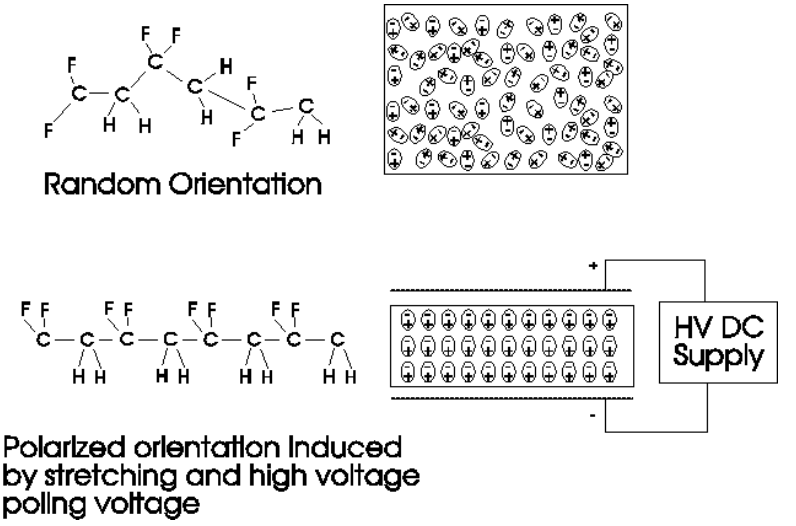

Figure 5. PVDF in alpha and beta phases.

The polymer chains in γ-PVDF have a structure between that of the α and β phases. The γ phase is ferroelectric but this form is experimentally hardly accessible. Formation typically requires high controlled temperature and high pressure, although recently, γ phase PVDF has been reported by melt re-crystallization using surface-energy-controlled top layers. The δ phase is a polar version of the α phase.

This kind of electrets can be polarized by application of electrical field to the material at room temperature or temperatures decreasing from a properly selected higher to lower value. Dipolar orientation can be achieved by the corona charging. In this case, the orientation is caused by the field of deposited charges[25].

5. AIMS OF THE STUDY

The general objective of this study was to solve the problem of using PVDF as a material for active element (balls) for twisting-ball display. The following tasks were performed:

1. Chemical functionalization of the surface of polyvinylidene difluoride (PVDF) particles to allow coating of the particles with a polystyrene layer.
2. Deposition of non-transparent hydrophilic alumina layer on the surface of PVDF particles to make the balls non-transparent and allow their coloring.
3. Coloring one hemisphere of the particles.
4. Poling the particles with the direction of the residual bias oriented the same way as the ball are colored
5. Assembly and testing of the functional display model.
6. Mathematical modelling of the behavior of the polarized balls in the changing electric field.

6. EXPERIMENTAL

6.1. Chemical functionalization of PVDF surface

PVDF particles with a diameter of 50 μm were tailored by Solvay Solexis (Italy) and had mean molecular masses of 31,500 or 315,000 for the two lots used in this study. In some experiments PVDF film (thickness 150 μm) was used. Before experiments the surface of the specimen was cleaned by washing with methanol and thereafter with CCl_4.

The used chemicals were purchased from Sigma Aldrich as ACS grade reagents and were used without additional purification, except styrene and acetonitrile. Styrene was distilled before experiments (18 mm Hg bp 44 °C) and stabilizer (hydroquinone) was removed by inhibitor removers 311322 (CAS 9003-70-7, Aldrich). No hydroquinone was detected in purified styrene by analysis of FT-IR spectra. Acetonitrile was dried over molecular sieves. $CuCl_2$ was purified by precipitation from glacial acetic acid, followed by washing with 2-propanol. CuCl was at the desired purity (99.995%). All salts were kept in vacuum desiccators.

Spectra of the surface-functionalized material as well as blank material were obtained by using the Attenuated Total Reflection Fourier Transform Infrared Spectroscopy (ATR FT-IR), using a Nicolet 6700 FT-IR spectrometer, calibrated against air before each series of experiments. Each spectrum was collected by cumulating 256 scans at a resolution of 4 cm^{-1} and 3 sample readings from different surface locations were recorded for eliminating the effects of micro-heterogeneity.

For scanning electron microscopy (SEM) study a small amount of powder was dispersed in the EpoThin® epoxy resin and cured in small molds at the room temperature. Slices with a thickness of 5μm were cut with an ultra-microtome LKB ULTROTOME® V, attached to the aluminium stubs and coated with the Au/Pd by ion sputtering to enhance the electrical conductivity. Investigation of the samples was carried out with a scanning electron microscope ZEISS EVO MA15 at 10 kV. For the given samples, each SEM image presented in this work is a representative among numerous images made on a different location on the sample.

Synthesis of the ATRP catalyst was made in the oxygen-free atmosphere by using dry-box equipment. Briefly: acetonitrile was bubbled for 30 minutes with dry argon gas and components were added to obtain the following solution: [TREN]=167 mM, [CuCl]=45 mM and [$CuCl_2$]=4.5 mM or 9.0 mM. This mixture was stirred for about 24 hours at 30 ºC in an argon atmosphere. The catalyst was air-tightly stored at 4ºC in a dry-box freezer.

ATRP reactions were made in the following mixtures: 2.5 ml styrene, 1.5 ml acetonitrile, 0.5 ml of catalyst in acetonitrile, 50 mg of PVDF samples (spherical particles or film, MW 315,000 or 31,000). Samples were stirred at 60ºC under an argon atmosphere. The reactions were stopped by rapid cooling

of the reaction mixture to room temperature and simultaneous exposure to air oxygen. In some test experiments copper salts and TREN were omitted from the reaction mixture and in these cases 0.5 ml of acetonitrile was added. In other test experiments copper salts were omitted and 0.5 ml of pure TREN was added, yielding its concentration 0.75 M in the reaction mixture. As we were interested in the covalently attached polystyrene, the particles were carefully washed three times with CCl_4 before spectroscopic measurements. This treatment was sufficient to remove traces of polystyrene and styrene from the surface of the material, as an increase in washing times had no effect on results. After this treatment FT-IR spectra were monitored and the absorbance at 699 cm^{-1} was taken as indication of the presence of the grafted polystyrene. This absorbance corresponds to the C-H out of plane bending in monoalkylated aromatics and comprises the strongest absorption band of styrene[26]. The amount of grafted polystyrene was estimated by comparison of this absorption with another absorption band for CF vibrations of PVDF at 1178 cm^{-1}[27], and the ratio of these band heights (CH/CF) was used for quantification of the amount of grafted polystyrene in arbitrary units, provisionally marked as the "grafting yield"[28].

6.2. Deposition of non-transparent hydrophilic alumina layer

Aluminium chloride hexahydrate ($AlCl_3 \times 6H_2O$), urea $CO(NH_2)_2$, trimethyl aluminium $Al_2(CH_3)_6$ (2M solution in hexane), lithium hydroxide and nitric acid were purchased from Sigma-Aldrich and were of the highest purity grade available. Milli-Q deionized water was used in experiments and for washing purposes. Before alumina coating the surface of the PVDF particles was grafted with a polystyrene layer, and details of this procedure and properties of the obtained product were described above.

Before alumina coating the polystyrene grafted PVDF particles were pre-treated with 5% LiOH solution in water for 24 h. LiOH was selected to use alkali of high purity. Thereafter, the particles were washed with water and dried in vacuum desiccators for 1 h, until a non-sticking powder was obtained. This powder contained 25–40 mg of water per gram of particles. This water was important for deposition of alumina precipitation centers. In separate experiments this remnant water was removed by processing particles in the vacuum of a freeze-dryer.

The obtained particles (3 g) were added into a 2M trimethyl aluminium solution in hexane (5 ml) and the mixture was gently stirred at room temperature under an argon atmosphere for 1 h. Thereafter, the particles were separated and washed with hexane and methanol and air-dried. The obtained particles were studied by SEM and were analyzed for the presence of aluminium on their surface.

After deposition of the alumina nucleation centers into the polystyrene layer, the layer of inorganic coating was added through precipitation of aluminium hydroxide from water solution of $AlCl_3$ at 90 °C as described by Idrissi-Kandri et al[32]. Briefly: 1 g of $AlCl_3 \times 6H_2O$ was dissolved in 50 ml of 2% NH_4OH solution and the pre-treated particles (5 g) were added. The mixture was heated up to 90 °C and at continuous stirring 20 ml of urea solution (45% in water) was added drop-wise for 6 h. Under these conditions $Al(OH)_3$ was precipitating and formed a uniform alumina layer. If gel formation was observed then the addition of urea was too fast. Finally the presence of the inorganic coating on the surface of PVDF particles was analyzed by using SEM in combination with FIB technology.

An EVO MA15 scanning electron microscope (Carl Zeiss) in combination with an energy-dispersive X-ray spectrometer INCA equipped with an X-Max 50 mm^2 detector (Oxford Instruments) was used for studying the morphology and chemical composition of particles. For obtaining line-scans of Al across the cross-section of particles acceleration voltage of 15 kV was used.

Secondly, surface morphology and cross-section images of the polymer particles were also studied with Dual Beam® equipment Helios NanoLab 600 having both high-resolution scanning electron microscope and scanning focused ion beam modes. For examination of surfaces the SEM was mainly used with 2 keV primary electrons and generated secondary electrons were registered with a through-the-lens detector.

For SEM measurements particles were mounted in EpoThin® epoxy resin (Buehler, USA) and slices with a thickness of 5 μm were cut with an ultra microtome LKB ULTROTOME® V. These slices were attached to the aluminium stubs with double-sided adhesive tape, and then the samples were coated with an Au/Pd mixture by ion sputtering to enhance electrical conductivity. However, in most cases application of the microtome distorted the shape of the particles. Therefore, for obtaining more adequate cuts of particles FIB technology was used. In these experiments a thin Pt protective coating was deposited by the electron and ion beams on the top surface of the particles. Thereafter, a part of the particles was sputtered away using FIB of 30 kV Ga^+ ions, and the cross-section surfaces were cleaned and polished by using the same FIB procedure. During both processes special software from the FEI Company was used.

6.3. Coloring of the particles

Black pigment was used from BIC ballpoint pens, black. Heat resistant polyimide tape was used as the high temperature adhesive. The surface of PVDF particles was modified in advance by coating with alumina layer, providing necessary optical properties (white color, reflective index), and simple offset printing technology was used (Fig. 6).

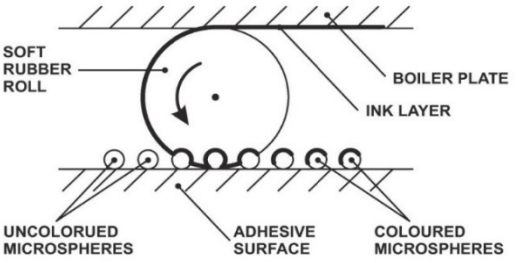

Figure 6. Scheme of coloring equipment.

Briefly, the balls were deposited onto a flat sticky surface, heat-resistant polyimide tape (Kapton, DuPont, USA), and black dye from BIC ballpoint pens was transferred to the surface of the particles using a soft rubber ink roller. The samples were kept for 24 hours in a dryer box at a temperature (45 °C) to fix the dye onto the surface of the particles, and thereafter the tape was directly taken into the polarization equipment (Fig. 7).

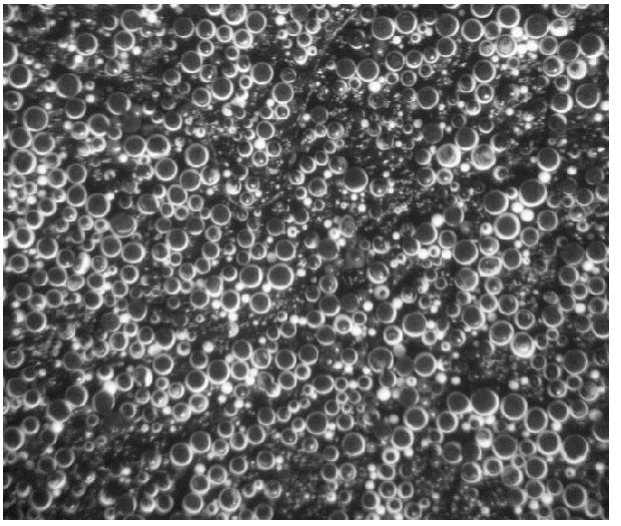

Figure 7. Bichromal balls on adhesive tape.

6.4. Poling of the particles

The corona charge method was selected for poling, as these treatments could be performed at room temperature and at atmospheric pressure in inert nitrogen atmosphere and these conditions were better suited for upgrade to an industrial scale process. Briefly: the particles were taken into the poling system with tape, and the sample was polarized with 7.5 kV during 60 minutes, distance from electrode to sample 5 mm (Fig. 8). After poling the particles were removed

from the carrier and repeatedly washed with hot (60 °C) hexane. The remnant solvent was removed in a vacuum.

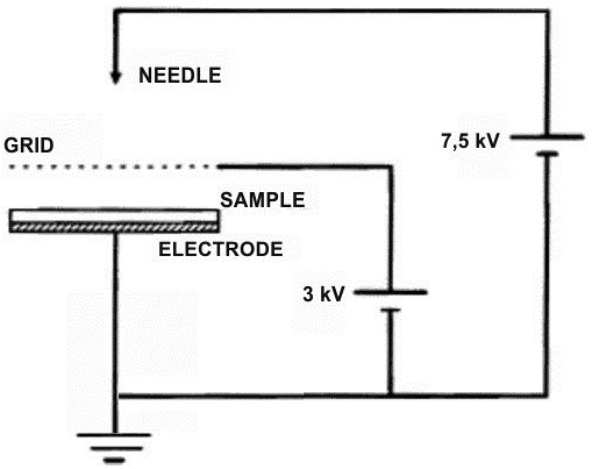

Figure 8. Scheme of the polarization equipment

6.5. Assembly of the display

The processed particles were encapsulated into a silicon elastomer host. The balls were first mixed with silicone (Sylgard 184) in its liquid state. The film of the silicone and balls mixture was formed and shaped with a "doctor blade 1/100" instrument. After this shaping the sample was heated during 240 minutes under nitrogen atmosphere, so the silicone was cured. After this step the film was treated with hexane during 60 minutes to obtain swelled material. The swollen film was placed between two electrodes. One of these electrodes was made of glass covered with ITO. The rectangular control voltage (±100 V) was applied to these electrodes and the movement of the particles was observed under a microscope.

7. RESULTS AND DISCUSSION

7.1. Chemical functionalization of PVDF surface

First-hand, by using $CuCl/CuCl_2$ complex with tris(2-aminoethyl) amine (TREN) as the catalyst, we were able to initiate polystyrene grafting on the surface of spherical particles of PVDF. A significant amount of covalently bound polystyrene was detected after one hour and results were similar for PVDF samples of Mw 31,000 and 315,000. Under the same conditions we were unable to observe crafting on PVDF film and only a significant extension of the reaction time revealed some covalently bound polystyrene. This can be explained by the larger net surface of the spherical particles if compared with the same mass of the pressed film. This difference certainly affected the rate of initiation of ATRP on PVDF surface. However, as we were focused on the grafting of spherical particles, this situation was rather satisfactory for our objectives and all further results described were obtained with spherical PVDF particles.

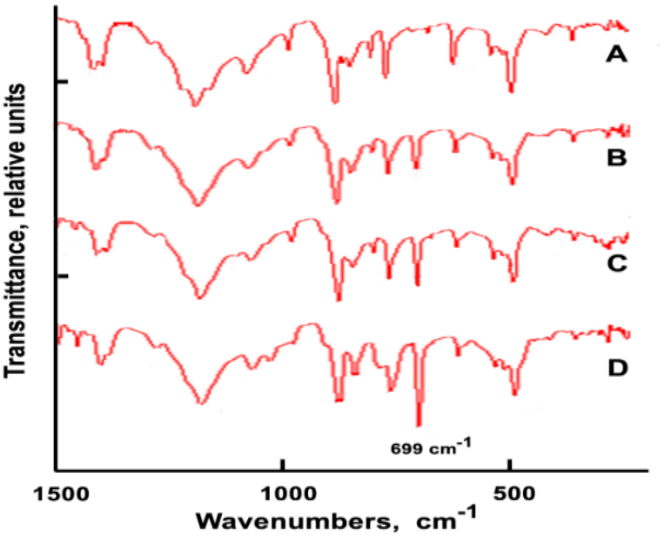

Figure 9. Changes in FT-IP spectra demonstrating PVDF grafting with polystyrene. A – PVDF particles before grafting, B, C and D – PVDF particles after grafting during 15 min, 30min and 60 min. The increase in the peak at 699 cm^{-1}, comprising the strongest polystyrene absorption band, demonstrated the development of polymer brushes on the surface of PVDF particles. Conditions of the reaction: 50 mg of PVDF particles, Mw 315000; [styrene]=4.8 mM; [AcN]=19.5 mM, [TREN]=19 mM, [CuCl]=5 mM; $[CuCl_2]$=0.5 mM, temp 60 °C

As mentioned, the covalently attached polystyrene was ascertained by ATR FT-IR technique[26] where separation of non-covalently bound polystyrene from grafted polymer has special importance. Therefore, a separate study of sample treatment conditions was made. First, the samples were extensively washed with CCl_4, which is an efficient solvent for polystyrene. Secondly, the grafted polymer samples were left after washing overnight in this solvent before spectra were measured. And finally, washing of samples was supported by treatment with ultrasound. After all these treatments the PVDF particles still retained characteristic polystyrene peaks in FT-IR spectra, confirming their covalent attachment with the surface.

The FT-IR spectra were also used to investigate the time-course of the grafting reaction. For example, if absorption at 699 cm^{-1} was absent in the initial PVDF particles (spectrum A, Fig. 9), this band was seen after progressing of the grafting reaction during 15, 30 and 60 min. (spectra B, C and D in Fig. 9).

Covalent attachment of polystyrene with PVDF significantly changed the morphology of the surface of the PVDF particles, as was observed by specimen probing with scanning electron microscopy (Fig. 10). It can be seen in Fig. 10A that the starting material possessed a rather smooth surface with no significant defects. Formation of polystyrene dendrites was clearly seen on the surface after treatment with styrene in the presence of ATRP catalyst (Fig. 10B). Moreover, it can be seen that the formed polystyrene "brushes" uniformly covered the surface of the particle.

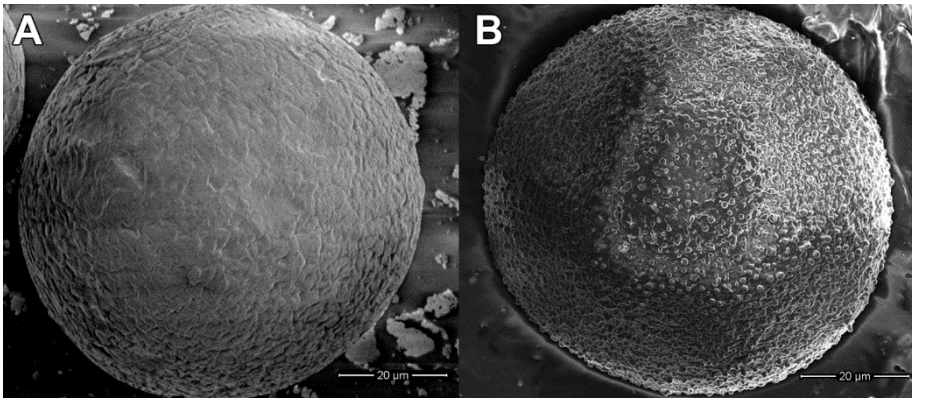

Figure 10. Change in morphology of the surface of a PVDF particles a result of the grafting procedure. A – PVDF particle before grafting reaction. B – PVDF particle after grafting during 4 h. Reaction conditions as described in the Experimental part. A closer look at these dendrites is given in Fig. 11.

Density of these "brushes" on the surface and their dimensions were increasing in time. The rate of growth was also dependent on the composition of the catalyst. Therefore, selection of the appropriate reaction time and other conditions can be used for obtaining the grafting polymer layer of the required

dimensions that has great significance for the technological application of the grafting process.

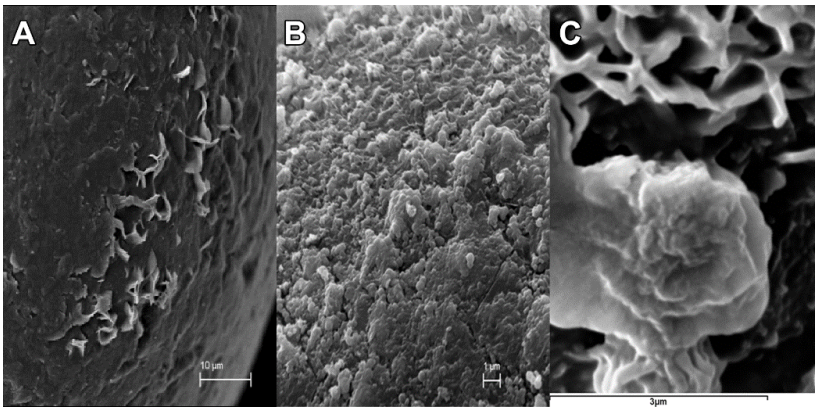

Figure 11. Polystyrene dendrites on the surface of PVDF particles at different magnifications.

Using the proposed spectroscopic method for determination of covalently bound polystyrene, the time-course of the grafting process was monitored at different reaction conditions. In Fig. 12, the influence of the different ratio of Cu(I) and Cu(II) concentration on the rate of the process was compared (Curves A and B). It can be seen that increasing of the content of $CuCl_2$ reduced the initial rate of the process.

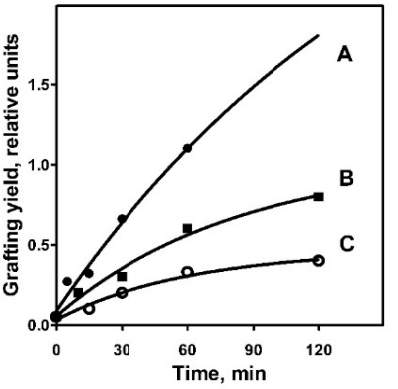

Figure 12. Time-course of a polystyrene covalent attachment to PVDF particles at 60 °C, assessed by the ratio of polystyrene and PVDF characteristic absorbencies at 699 and 1178 cm^{-1}, respectively. Different amounts of Cu(I)Cl and $Cu(II)Cl_2$ were used in the experiments.
Curve A: [CuCl]=5 mM; [$CuCl_2$]=0.5 mM, [TREN]=19 mM
Curve B: [CuCl]=5 mM; [$CuCl_2$]=1 mM, [TREN]=19 mM
Curve C: No copper salts, [TREN]=760 mM.

This is in agreement with the general ATRP mechanism, where equilibrium between different oxidation states of the copper catalyst should determine the concentration of reactive spices (the amount of formed initiator sites) and therefore should also govern the initial rate of the catalyzed reaction. This situation was illustrated by reaction scheme in Fig. 13, where formation of the initiator sites through homolytic cleavage of C-F bonds was assumed. This initiation process was catalyzed by Cu(I) salt, and concentration of this catalyst, in turn, was regulated through its equilibrium with Cu(II) salt.

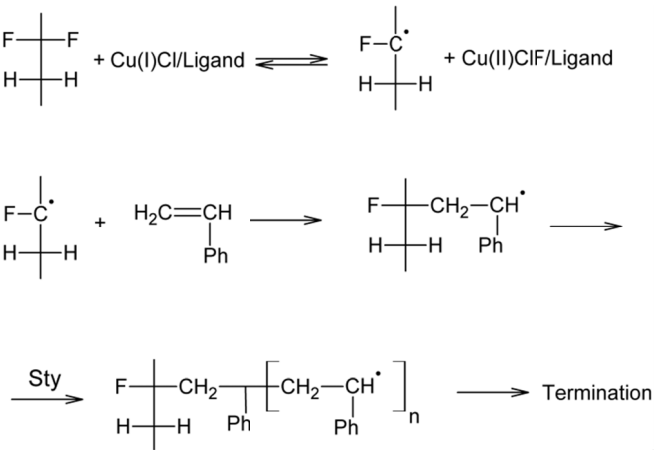

Figure 13. Formation of radical initiator sites through homolytic cleavage of C-F bonds, followed by styrene polymerization starting from these radicals formed on the PVDF surface. The initiation step was catalyzed by Cu(I)Cl/ligand complex following the ATRP mechanism.

Secondly, it can be seen in Fig. 13 that the polymerization reaction levelled off after a certain time interval, and the time-course of the process was modelled by an exponential function. Interestingly, the half-life of both ATRP processes was close, although the spans as well as initial rates were different. Without going deeply into the kinetics of these processes, it can be mentioned that these regularities allow controlling the mass and dimensions of the grafted polystyrene layer that was an important feature of the discussed ATRP technology.

However, in addition to the conventional ATRP reaction described above, covalent attachment of polystyrene to PVDF surface was also observed in experiments, where copper catalyst was omitted from the reaction mixture, but a large amount of the catalytic ligand TREN was added (760 mM). Evidently, this reaction was not initiated by the ATRP mechanism. To explain the role of TREN in this reaction, a hypothetical mechanism of this process was suggested as shown in Fig. 14. In the formulation of this mechanism we considered that TREN is a rather strong base, which can initiate CH acid dissociation and carbanion formation from PVDF chain, and thus initiate anionic polymerization

of styrene. Formation of carbanion through CH bond heterolytic dissociation should be strongly supported by neighboring fluorine atoms in PVDF structure, as is typical for influence of fluorine atoms on C-H bond strength in structural fragments F-C-C-H[29].

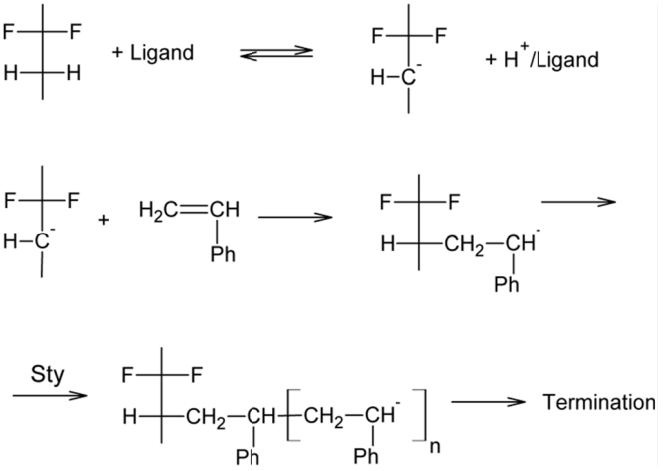

Figure 14. Formation of anionic initiator sites through C^-H bond heterolytic dissociation, assisted by the basic ligand and supported by neighboring fluorine atoms in PVDF structure, and followed by styrene polymerization starting from these carbanion sites formed on the PVDF surface.

After initiation, the polymerization reaction may lead to the formation of polystyrene brushes on PVDF surface, detected in FT-IR spectrum. However, a difference compared to the ATRP mechanism is that this putative carbanion formation mechanism has not been described and studied in detail, although this may open some new perspectives for the grafting of fluorinated polymeric materials.

7.2. Deposition of non-transparent hydrophilic alumina layer

The first step of the proposed alumina deposition process was based on the reaction between trimethyl aluminium and water:

$$Al_2(CH_3)_6 + 3\ H_2O \rightarrow Al_2O_3 + 6CH_4.$$

Previously this reaction has been used for growing alumina film in a vacuum[30]. However, in the present study we transferred this procedure into liquid phase, using a 2M solution of trimethyl aluminium in hexane as a reaction medium. The polystyrene grafted PVDF particles were added into this

reaction medium in an argon atmosphere to avoid spontaneous inflammation of the reaction mixture. Before this step, however, the particles were treated with an alkali solution, washed with water and dried in a vacuum. This drying procedure was purposely incomplete, and a minor amount of water was left within the brushy polystyrene layer of the grafted particles. This water reacted with trimethyl aluminium and the formed alumina was located within and around the polystyrene structures. Importantly, if the traces of water were completely removed, alumina formation on the polymer surface was not observed.

The presence of alumina in the regions covered with polystyrene brushes was confirmed by a combination of SEM and an electron probe micro-analyzer and the results of this analysis were shown in Fig. 15.

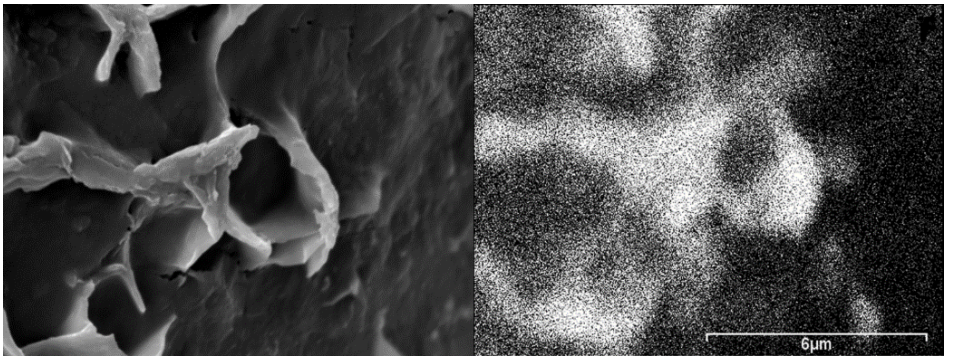

Figure 15. Comparison of surface topography (left panel, SEM) and aluminium distribution at the same place (right panel, X-ray micro-analyzer) on a polystyrene-grafted PVDF particle after its treatment with trimethyl aluminium. The chemical map (right panel) was presented in white-to-black scale with its white end corresponding to the maximum aluminium content. The grafted polystyrene "brushes" (white structures in the left panel) were the main sites for aluminium deposition, while practically no aluminium was observed on the PVDF surface (black surface, left panel).

It can be seen that most of the aluminium was indeed distributed across the polystyrene structures formed during the crafting process, and only traces of aluminium were detected on the PVDF surface that was not covered with polystyrene. As a result of this directed deposition procedure a very flimsy layer of alumina was obtained, as can be seen from the results of the X-ray line scan (Fig. 16) of the cross-section of the coated particle. The surface layer of this particle contained approx. 120 ppm of aluminium.

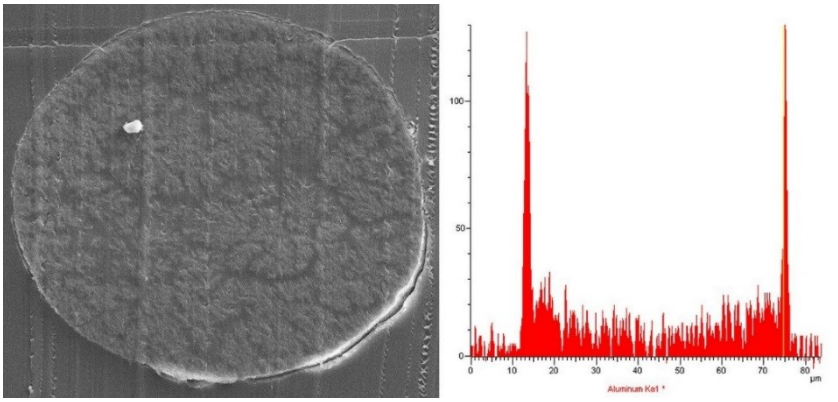

Figure 16. SEM picture of a cross-section of a polystyrene-grafted PVDF particle covered with a thin layer of alumina deposited during the first step of the coating process. The presence of aluminium atoms on the surface of the particle was determined by X-ray line scan of the cross-section of this particle. The maximum aluminium content on the edges of the slice was 120 ppm. The spherical particle was slightly damaged by using a microtome for cutting the sample. The investigation of the electrode surfaces and local processes by structure-sensitive probing techniques has become an adsorbate layers to some specific structural features in the micrometer layers.

The size and structure of the alumina particles formed in the polystyrene layer were not specified in this study. However, by analogy with other results it could be suggested that in the absence of the excess of water the formation of alumina crystals[30] or their conglomerates[31] occurred. In any case, the formed alumina centers were effective for priming the formation of an aluminium hydroxide layer if precipitated from the bulk solution.

During the second step of the process the particles were covered with a robust layer of inorganic material that was necessary to meet the needs of our technology. This layer was obtained through precipitation of aluminium hydroxide from water solution of $AlCl_3$. Although many methods of aluminium hydroxide synthesis have been described in literature[32][22][33], it was found that the main criterion of applicability of this reaction for our needs was the slowness and controllability of the process, as it was absolutely important to avoid formation of aluminium hydroxide gel in the bulk solution or its massive precipitation during the process. These side effects were minimized, if the high temperature decomposition of urea was used to initiate aluminium hydroxide formation[32] from the $AlCl_3$:

$$CO(NH_2)_2 + 4H_2O = CO_2 + 2NH_4OH$$

$$AlCl_3 + 3NH_4OH = Al(OH)_3 + 3NH_4Cl$$

The conditions of this synthetic procedure were optimized and a uniform coating of PVDF particles was obtained. Initially the inorganic layer obviously consisted of aluminium hydroxide, as precipitation was made from the water solution of $AlCl_3$. For converting this precipitate into a more compact inorganic layer, the material was dried in a vacuum at 90 °C until non-sticky particles were formed.

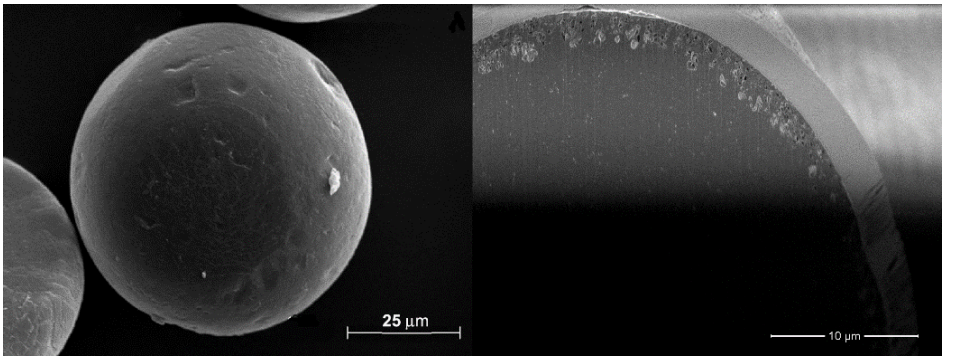

Figure 17. SEM pictures of the alumina-coated PVDF particles (left panel) and a cross-section of the coated particle (right panel). An inorganic layer of approx. 2 µm thickness was obtained through the two-step deposition procedure, and was integrated with the particle main body through the porous ("brushy") polystyrene layer grafted to the PVDF surface. The slice shown in the right panel was prepared by using the FIB procedure as described in the experimental section.

In Fig. 17 the SEM picture of the obtained particles was shown, including a cross-section of one particle. It can be seen that a uniform and dense inorganic coating was obtained. Below this layer a slightly porous polymer layer can be seen that is most likely the contact area of the PVDF surface and the grafted polystyrene entrained into the alumina layer.

7.3. Poling of the particles

The following methods were used for testing of the poled PVDF particles: polarization measurements, calorimetric analysis of particle melting, and observation of particle movement in the electric field.

Polarization measurements were made with poled particles encapsulated in silicone glue using Premier II (Radiant Technologies Inc.) equipment (Sawyer–Tower method) and an APC d33 meter (APC International, Ltd.). The silicone films were placed on the sample holder and the polarization value was measured at increasing electric field. The results revealed a clear hysteresis loop in the case of the polarized material (Fig. 18), indicating that the material had acquired polarization. If testing non-poled material a straight line appeared. However, due to the non-uniformity of the samples the hysteresis curves were not

saturated and the maximum polarization value was not obtained, but still the polarization of the particles was evident.

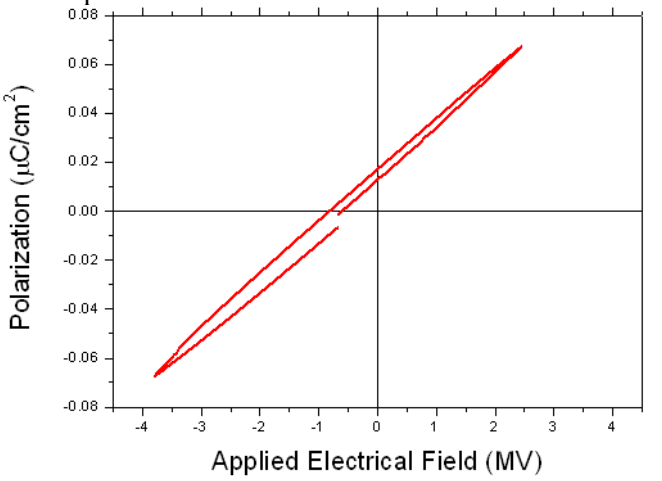

Figure 18. Hysteresis measurements of the silicone film with the encapsulated microparticles

In the *differential scanning calorimetric* (DSC) measurements the heat flow of the poled and non-poled material was measured in the temperature range from 20 to 170 °C (Microcal LLC, UK). The obtained results are illustrated in Fig. 18. The DSC curves clearly show the difference of the endothermic peaks of the poled and non-poled samples at the melting temperature of the material. The poled β-phase PVDF samples presented higher melting entropy, and since both the melting peaks show a similar melting enthalpy, the melting temperature of the poled samples (160 °C) was lower than that of the non-poled samples (162 °C). This result confirmed the formation of some amount of β phase PVDF in the processed material.

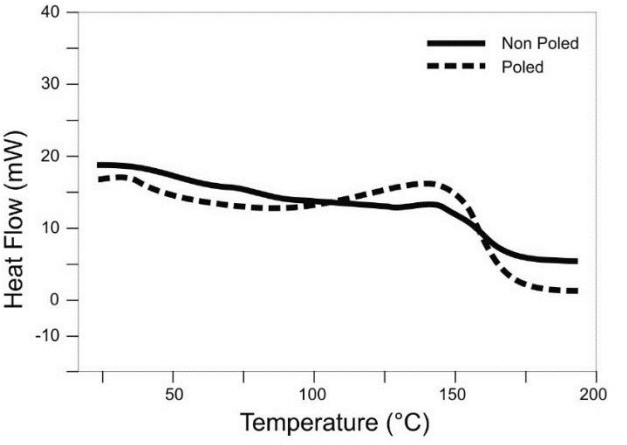

Figure 19. Snapshots of the “white” and “black” states of the display element used for demonstration of the twisting balls.

Movement of particles was monitored under an optical microscope (20–100×), obtaining snapshots of the display element (see Fig. 1). This display element was obtained as follows. The poled and colored particles were encapsulated in a silicone elastomer layer. The balls were first mixed with liquid silicone Sylgard 184 at a ratio of 1 ml of particles to 1 ml of silicone mix. From this mixture of balls and elastomer, a thin film was made by using a “doctor blade 1/100” instrument (Max Daetwyler Corporation). The film was heated during 240 minutes at 90 °C in air, so that the silicone was cured. Thereafter, the film was kept in a closed cuvette under a hexane layer for 60 minutes. After swelling of the film, its volume increased by 10–15%. The swollen film was placed between two control electrodes, one of which was glass covered with ITO (indium tin oxide). The cap between the electrodes was sealed by using a two-component epoxy wax. A rectangular control voltage (±100 V) was applied between the electrodes and the rotational motion of the particles was observed and snapshots were obtained at two polarization states (Fig. 20). It can be seen that practically all particles within the window were able to follow the change of the polarity of the control voltage.

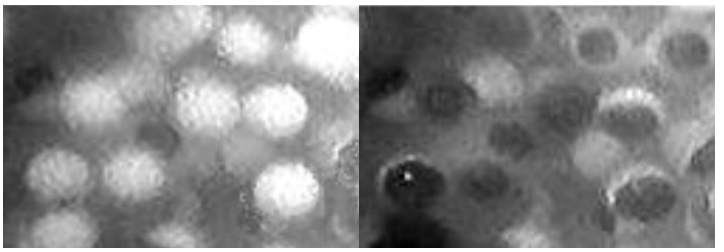

Figure 20. Snapshots of the “white” and “black” states of the display element used for demonstration of the twisting balls.

8. MATHEMATICAL MODELING OF THE BEHAVIOR OF THE POLED PARTICLES

8.1. Ball in the cavity

Each ball of the twisting-ball display is an electrical dipole[9] and is placed in the cavity filled with dielectric fluid. The width of the cavity is 10–30% greater than the diameter of the balls. When the polarity of the control voltage is changed, the position and orientation of the balls change and one or other of their colored sides is exposed to the viewer. The balls are made by first melting or heating a suitable dielectric material and then allowing it to cool in a powerful electrostatic field. The polar molecules of the dielectric align themselves in the direction of the electrostatic field, producing a permanent electrostatic bias. Each ball has a monopolar electrical charge and bipolar charge. When the control voltage is constant or zero, the ball is "glued" to the wall of the cavity due to the electrostatic forces. When the polarity of the control voltage changes, the ball begins to move towards the opposite wall of the cavity. A schematic view of the situation is given in Fig. 21.

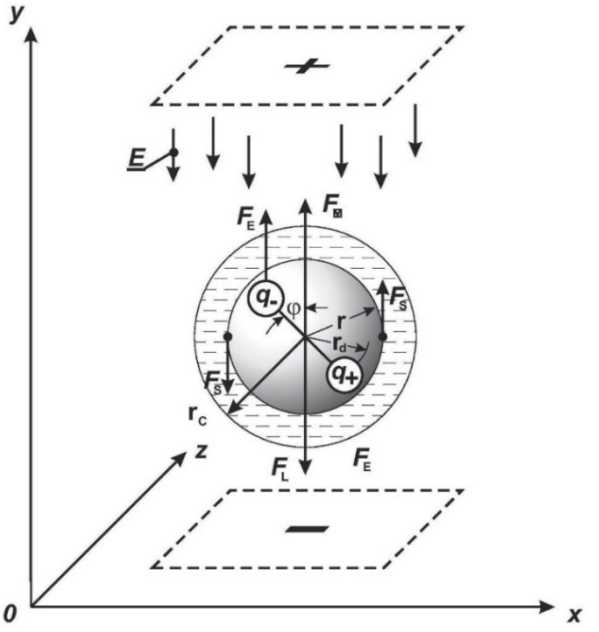

Figure 21. Schematic view of dichromatic ball in cavity

For the radius of the cavity we have

$$r_C = \alpha \cdot r \tag{1}$$

with some α>1. For the radius of the dipole we have

$$r_{\mathrm{D}} = \frac{r}{2} \tag{2}$$

The physical bounds for ball shift are $0 \le y(t) \le 2(r_{\mathrm{c}} - r)$. For the simulation, we apply the electric force in the form of a periodic rectangle function $U(t)$ with period T and amplitude $\pm U_{\mathrm{c}}$.

The integral Lambertian luminance of this kind of display very complicated and in this work a model of integral luminance was proposed. This model considers the stochastic placement of the particles, and diffraction, refraction and reflection of light on different surfaces inside the display. However, here we use a very simplified model as we need only a relative value of the luminance to describe the performance of the display, not the absolute one. We presume that all the particles are placed in a regular way (see Fig. 22). We presume that the reflectance of the black side of a particle is 0 and of the white side is 100%. For modelling of the reflection, the plane of the display is divided into hexagons with cavities inside these, as shown in Fig. 22.

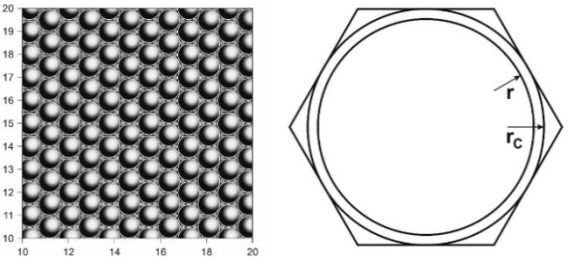

Figure 22. The plane of display divided into hexagons.

The area of the visible size of the particle is

$$S_1 = \pi \cdot r^2 \tag{3}$$

The area of the corresponding a hexagon is

$$S_2 = \frac{3r_C^2}{\sin 60^o} = \frac{2}{\sqrt{3}} r_C^2 = \frac{2}{\sqrt{3}} n^2 \cdot r^2 \tag{4}$$

The black area of the ball exposed to the viewer is[34]

$$S_3 = \frac{\cos\varphi + 1}{2} S_1 \tag{5}$$

The relative luminance is

$$L = \frac{S_2 - S_3}{S_2} = 1 - \frac{\sqrt{3}}{4} n^2 \cdot (\cos\varphi + 1) \tag{6}$$

The illumination depends on the rotation angle of the bichromal balls inside of the cavity. This dependence is depicted in Fig. 23, showing the rate of dark area as a function of rotation angle.

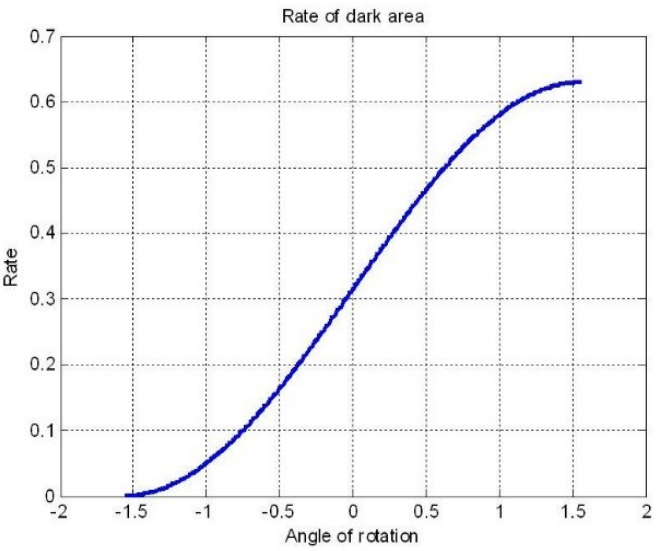

Figure 23. Rate of dark visible area of the ball.

8.2. Source data

Most of the source data have technological background.
The median radius for achieving sufficient image quality (150 dpi) is

$$r = 25 \times 10^{-6} \text{ m}$$

A larger thickness of the elastomer sheet increases the contrast of the image. At the same time, increasing the thickness means using higher control voltages, which is inadvisable. Optimal thickness achieved experimentally is equal to 3 diameters of the ball:

$$R_D = 150 \times 10^{-6} \text{ m}$$

The coefficient of expansion of the elastomer sheet n can be between 1.1 and 1.5. In our work we use

$$n = 1.2$$

Possible control voltage is different for different backplane units. Ideally (using standard solutions)

$$U_c = 15 \text{ V}$$

We observe the maximum possible control voltage for commercial backplanes:

$$U_c = 100 \text{ V}$$

The density of PVDF [35] is given by

$$\rho = 1.75 \times 10^3 \text{ kg/m}^3$$

The monopolar charge of the particle and the dipole charge can be measured experimentally. In our experiments, the dipole charge can be changed by changing the polarization parameters and the monopolar charge can be simply controlled using nonpolar surfactants dissolved in the carrier liquid:

$$q_D = 1 \times 10^{-18} \text{ C to } 1 \times 10^{-16} \text{ C}$$

$$q = 1 \times 10^{-18} \text{ C to } 1 \times 10^{-16} \text{ C}$$

Hexane is used as a carrier liquid. The viscosity[36] of hexane is

$$\acute{\eta} = 3 \times 10^{-4} \text{ N} \times \text{s/m}^2$$

8.3. Mathematical model

The ball inside the cavity accelerates at first and reaches a stable velocity determined by the diameter of the ball and the viscosity of the carrier liquid. Without loss of generality we can assume that the equilibrium state of a ball in the cavity is at the cavity wall. Each ball has a monopolar electrical charge and bipolar charge; and when the control voltage is constant or zero, the ball is "glued" to the wall due to the electrostatic forces[9]. If the control voltage changes, the ball begins to move towards the opposite wall of the cavity. We neglect the influence of gravity and buoyant force because of their smallness in comparison with the electrostatic force and viscous drag. The shift $y = y(t)$ of the ball is described by the differential equation

$$\frac{d^2 y}{dt^2} - \frac{F_E - F_L}{m} = 0 \tag{7}$$

Here, F_E is an electrostatic force:

$$F_E = E \cdot q \tag{8}$$

F_L is a viscous drag. We presume that the velocity of the ball is relatively low and we can use Stokes' law to determine the resistance of the fluid:

$$F_L = d \cdot v = 6 \cdot \pi \cdot \eta \cdot r \cdot \frac{dy}{dt} \tag{9}$$

The mass m of the particle is

$$m = \rho \cdot V = \frac{4}{3} \cdot \pi \cdot \rho \cdot r^3 \tag{10}$$

Although in real systems the magnitude of the electric field varies across the thickness of the material due to the difference of the permittivity of silicone, carrier liquid and ball material, we accept a simplification:

$$E = \frac{U}{s} \tag{11}$$

The resulting differential equation is

$$\frac{d^2y}{dt^2} + \frac{9 \cdot \eta}{2 \cdot \rho \cdot r^2} \cdot \frac{dy}{dt} - \frac{3 \cdot U \cdot q}{4 \cdot \pi \cdot s \cdot \rho \cdot r^3} \tag{12}$$

The simulated trajectory of the ball governed by the differential equation (8) is shown in Fig. 24. The initial conditions are $y(0) = y'(0) = 0$.

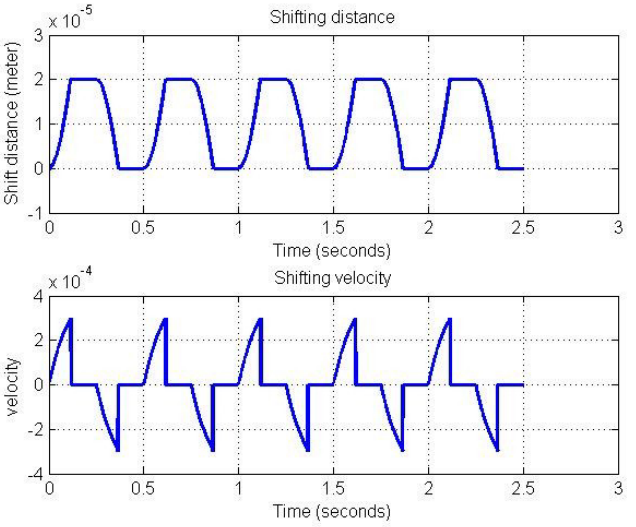

Figure 24. Movement of the ball in cavity; q=6 x 10^{-16}C

Rotation of the ball inside the cell cavity as a result of the outer electrical field can be described through the balance relation

$$M_J + M_S + M_E = 0 \tag{13}$$

where M_J is the inertial torque:

$$M_J = -J \frac{d^2}{dt^2} \tag{14}$$

J is the moment of inertia of the ball:

$$J = \frac{2}{5} m \cdot r^2 = \frac{8}{15} \pi \cdot \rho \cdot r^5 \tag{15}$$

M_S is the viscous torque:

$$M_S = -2\pi \cdot \eta \cdot r^4 \cdot \frac{d}{dt} \int (\sin\alpha)^3 d\alpha = -\frac{8}{3} \pi \cdot \eta \cdot r^4 \frac{d}{dt} \tag{16}$$

and M_E is the electrostatic torque:

$$M_E = 2r_D \cdot q_D \cdot E \cdot \sin\varphi \tag{17}$$

The resulting differential equation describes the rotation of the ball:

$$-\frac{8}{15} \pi \cdot \rho \cdot r^5 \frac{d^2\varphi}{dt^2} - \frac{8}{3} \pi \cdot \eta \cdot r^4 \frac{d\varphi}{dt} + \frac{r \cdot q_D \cdot U \cdot \sin\varphi}{S} = 0 \tag{18}$$

The magnitude of rotation depends on several parameters. Fig. 25 shows a sample movement of a ball free of the cavity.

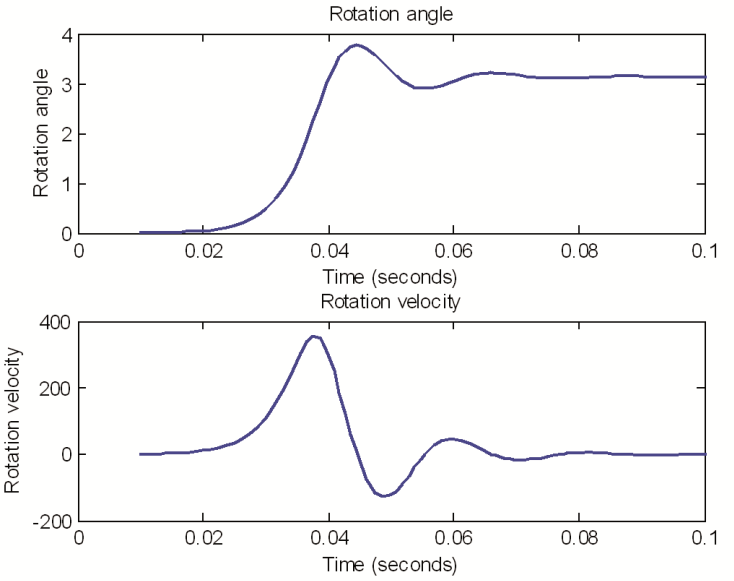

Figure 25. Sample plot of ball rotation.

If the ball is in the cavity, physical boundaries are applied. When the polarity of the control voltage is changed, the ball begins to move towards the opposite wall of the cavity. The rotation stops at the moment when the ball reaches opposite wall and ball does not obtain the equilibrium state as we saw on Figure 25. The changes of the angle and velocity of ball rotation corresponding to this situation with different electrical parameters of the ball are shown in Fig. 26–28.

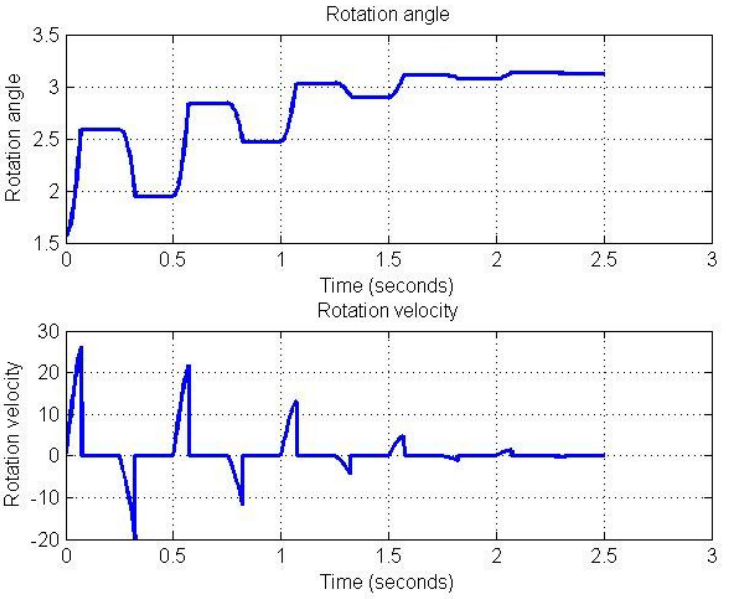

Figure 26. Rotation angle and velocity of the ball in cavity ($q_D = 1\times10^{-18}$ C)

In Fig. 26 we see that in the case of small dipole charge the ball performs some incomplete rotation cycles and stops in some fixed angle.

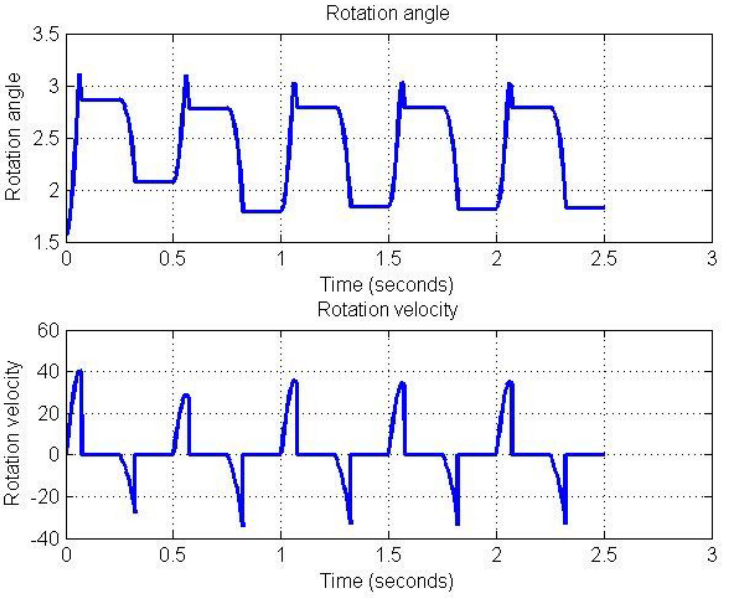

Figure 27. Rotation angle and velocity of the ball in cavity ($q_D = 2\times10^{-18}$ C)

In Fig. 27 the ball has nearly optimal dipole charge, other parameters remain unchanged. We see that in this case the ball rotation intends towards some complete rotation cycle. If control voltage changes, the ball rotates nearly 180° and exposes right, black or white size to the observer. Display works as expected.

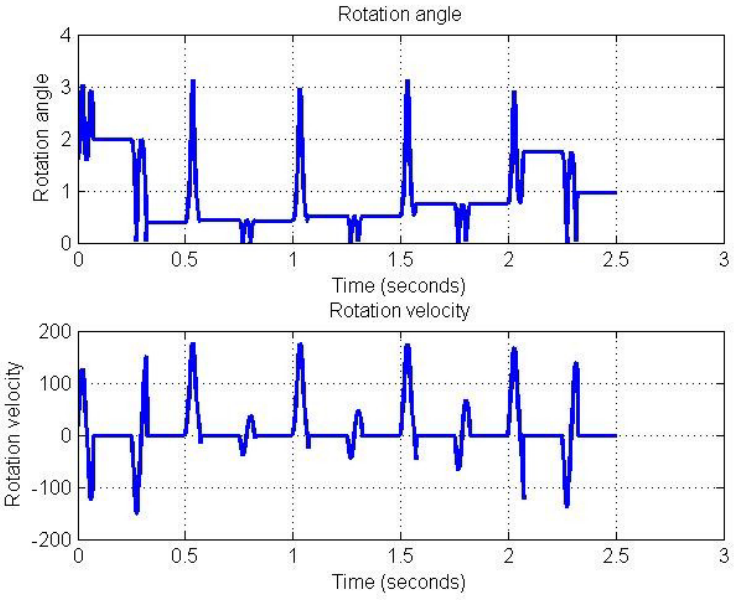

Figure 28. Rotation angle and velocity of the ball in cavity ($q_D = 1 \times 10^{-16}$ C)

In Fig. 28 we see that when dipole charge of too big, over some critical value, then the uniform rotation cycles of the ball are lost and ball performs random rotations and stops in unpredictable states.

9. CONCLUSIONS

In this study we demonstrated the possibility of using PVDF as a material of the active element for twisting-ball displays. The process of functionalization and covering the PVDF particles' surface, and poling and coloring the particles was proposed and tested in the case of a functional model of the display element.

It was found that the ATRP reaction can be used for chemical functionalization and grafting of spherical PVDF particles with polystyrene. The copper catalyst, consisting of mixture of CuCl and $CuCl_2$ in complex with TREN was used for the initiation of the process. The rate of the grafting process as well as the properties of the polystyrene layer could be governed through variation of the ratio of copper salts used, but also by variation of the reaction time. These results were in agreement with the general mechanism of ATRP reactions, and provided a good possibility for optimization of the surface functionalization technology. In addition another possibility for PVDF surface grafting was discovered, probably including the base-catalyzed carbanion formation and the following anionic polymerization of styrene on the surface of the particles.

To improve the opto-mechanical properties of PVDF particles it was important to obtain uniform coating of the particles by alumina layer. This objective was reached by developing the two-step alumina deposition procedure, where the preliminary functionalization of the PVDF surface with polystyrene brushes was the most critical step. The presence of this polystyrene layer was used for the initial deposition of alumna particles into the polystyrene structure by using hydrolysis of trimethyl aluminium, followed by the controlled alumina precipitation procedure from water solution.

One hemisphere of the alumina coated particles was colored and their electrostatic bias was generated by using the corona charge. Thereafter, the PVDF “balls” used for building of the model display element, to demonstrate voltage controlled movement of the particles.

Finally, a mathematical model that described the behavior of an elementary cell of the twisting-ball display was introduced that gave a theoretical insight into the ball shift and rotation movements, and allowed description of the dependence between the luminance and rotation time in the case of different physical parameters of the active element (poled ball).

Taken together, the study confirmed that PVDF might be a proper material for the preparation of active elements of a twisting-ball display

10. REFERENCES

[1] N. Sheridon, "Twisting ball panel display," *US Pat. 4,126,854*, 1978.

[2] N. K. Sheridon, "Gyricon Materials for Flexible Displays," in *Flexible Flat Panel Displays*, G. P. Crawford, Ed. John Wiley & Sons, Ltd, 2005.

[3] J. Liiv, "Active optical element, method of producing the same." *US Pat 8,383,010,* 2013.

[4] F. S. Foster, K. A. Harasiewicz, and M. D. Sherar, "A history of medical and biological imaging with polyvinylidene fluoride (PVDF) transducers", *IEEE Trans. Ultrason. Ferroelectr. Freq. Control*, vol. 47, no. 6, pp. 1363–71, Jan. 2000.

[5] J. Liiv, I. Zekker, D. Panov, V. Sammelselg, T. Tenno, and J. Järv, "Chemical functionalization of a polyvinylidene fluoride surface," *Polym. J.*, vol. 45, no. 3, pp. 313–317, Aug. 2012.

[6] J. Liiv, D. Panov, T. Tenno, and J. Järv, "Alumina coating of polyvinylidene fluoride (PVDF) surface in liquid phase," *Surf. Eng.*, p. 1743294414Y.000, Feb. 2014.

[7] J. Liiv, A. Mashirin, T. Tenno, and P. Miidla, "Mathematical modeling of performance of the twisting-ball display," *Proc. Est. Acad. Sci.*, 2014.

[8] N. K. Sheridon, E. A. Richley, J. C. Mikkelsen, D. Tsuda, J. M. Crowley, K. A. Oraha, M. E. Howard, M. A. Rodkin, R. Swidler, and R. Sprague, "The gyricon rotating ball display," *J. Soc. Inf. Disp.*, vol. 7, no. 2, pp. 141–144, 1999.

[9] J. M. Crowley, N. K. Sheridon, and L. Romano, "Dipole moments of gyricon balls," *J. Electrostat.*, vol. 55, no. 3–4, pp. 247–259, Jul. 2002.

[10] N. Durand, B. Ameduri, K. Takashima, K. Ishida, S. Horie, and Y. Ueda, "Vinylidene fluoride telomers for piezoelectric devices," *Polym. J.*, vol. 43, no. 2, pp. 171–179, Dec. 2010.

[11] E. Yamada, A. Nishioka, H. Suzuki, G. Murasawa, K. Miyata, T. Koda, and S. Ikeda, "Effect of Blended Montomollironite on Crystallization of Poly(vinylidene fluoride)," *Polym. J.*, vol. 41, no. 5, pp. 383–388, 2009.

[12] M. K. Tiwari, I. S. Bayer, G. M. Jursich, T. M. Schutzius, and C. M. Megaridis, "Poly(vinylidene fluoride) and Poly(ethyl 2-cyanoacrylate) Blends through Controlled Polymerization of Ethyl 2-Cyanoacrylates," *Macromol. Mater. Eng.*, vol. 294, no. 11, pp. 775–780, Nov. 2009.

[13] M. G. Buonomenna, L. C. Lopez, P. Favia, R. D'Agostino, A. Gordano, and E. Drioli, "New PVDF membranes: The effect of plasma surface modification on retention in nanofiltration of aqueous solution containing organic compounds," *Water Res.*, vol. 40, no. 19, pp. 4309–4316, 2007.

[14] R. Crowe and J. P. S. Badyal, "Surface modification of poly(vinylidene difluoride) (PVDF) by LIOH," *J. Chem. Soc. Chem. Commun.*, no. 14, pp. 958–959, 1991.

[15] N. Chakrabarti and J. Jacobus, "The Chemical Reduction of Poly(tetrafluoro-ethy1ene)," vol. 2, no. 1, pp. 3011–3014, 1988.

[16] L. Kavan, P. Janda, and J. Weber, "Surface modification of poly (tetrafluoro-ethylene) by magnesium amalgam," *J. Mater. Sci.*, vol. 6, pp. 879–885, 2001.

[17] K. Matyjaszewski and J. Xia, "Atom Transfer Radical Polymerization," *Chem. Rev.*, vol. 101, no. 9, pp. 2921–2990, Sep. 2001.

[18] K. Matyjaszewski, P. J. Miller, N. Shukla, B. Immaraporn, A. Gelman, B. B. Luokala, T. M. Siclovan, G. Kickelbick, T. Vallant, H. Hoffmann, and T. Pakula,

"Polymers at Interfaces: Using Atom Transfer Radical Polymerization in the Controlled Growth of Homopolymers and Block Copolymers from Silicon Surfaces in the Absence of Untethered Sacrificial Initiator," *Macromolecules*, vol. 32, no. 26, pp. 8716–8724, Dec. 1999.

[19] Y. Chen, D. Liu, and Q. Deng, "Atom transfer radical polymerization directly from poly (vinylidene fluoride): Surface and antifouling properties," *J. Polym.Sci.*, vol. 44, pp. 3434–3443, 2006.

[20] D. Mishra, S. Anand, R. Panda, and R. Das, "Statistical optimization of conditions for the hydrothermal precipitation of boehmite," *Hydrometallurgy*, vol. 58, no. 2, pp. 169–174, Dec. 2000.

[21] T. Sugimoto, *Monodispersed Particles*. Amsterdam: Elsevier, 2001.

[22] H. Willard and N. Tang, "A Study of the Precipitation of Aluminum Basic Sulfate by Urea1," *J. Am. Chem. Soc.*, no. 3, pp. 1190–1196, 1937.

[23] G. M. Sessler, Ed., *Electrets*, 3th ed. Berlin: Springer-Verlag, 1987.

[24] M. Li, H. J. Wondergem, M.-J. Spijkman, K. Asadi, I. Katsouras, P. W. M. Blom, and D. M. de Leeuw, "Revisiting the δ-phase of poly(vinylidene fluoride) for solution-processed ferroelectric thin films.," *Nat. Mater.*, vol. 12, no. 5, pp. 433–8, May 2013.

[25] J. M. Kenney and S. C. Roth, "Room temperature poling of poly(vinylidene fluoride) with deposited metal electrodes," *J. Res. Natl. Bur. Stand. (1934).*, vol. 84, no. 6, p. 447, Nov. 1979.

[26] J. Masson, L. Pelletier, and P. Collins, "Rapid FTIR method for quantification of styrene-butadiene type copolymers in bitumen," *J. Appl. Polym. Sci.*, vol. 79, no. 6, January 2000, pp. 1034–1041, 2001.

[27] R. Simoes, "Tailoring the structural properties of PVDF and P(VDF-TrFE) by using natural polymers as additives," *Polym. Eng.* vol. 49, no. 10, 2009.

[28] M. Albores-Velasco and E. Lopez, "Quantification of Polystyrene Acylation by IR Spectroscopy. An Experiment on Polymer IR Analysis," *J. Chem. Educ.*, vol. 74, no. 5, pp. 551–552, 1997.

[29] D. R. Burgess and M. R. Zachariah, "Thermochemical and chemical kinetic data for fluorinated hydrocarbons," *Prog. En. Combust. Sci*, vol. 21, no. 5, pp. 453–529, 1995.

[30] C. Soto and W. T. Tysoe, "The reaction pathway for the growth of alumina on high surface area alumina and in ultrahigh vacuum by a reaction between trimethyl aluminum and water," *J. Vac. Sci. Technol. A Vac. Surfaces Film.*, vol. 9, no. 5, pp. 2686–2695, 1991.

[31] Y. Li, X.-Y. Yang, G. Tian, A. Vantomme, J. Yu, G. Van Tendeloo, and B.-L. Su, "Chemistry of Trimethyl Aluminum: A Spontaneous Route to Thermally Stable 3D Crystalline Macroporous Alumina Foams with a Hierarchy of Pore Sizes," *Chem. Mater.*, vol. 22, no. 10, pp. 3251–3258, May 2010.

[32] N. Idrissi-Kandri, A. Ayral, C. Guizard, E. H. El Ghadraoui, and L. Cot, "Synthesis, characterization and first application of new alumina hydrosols," *Mater. Lett.*, vol. 40, no. 2, pp. 52–58, Jul. 1999.

[33] P. Mishra, "Low-temperature synthesis of a-alumina from aluminum salt and urea," vol. 55, no. September, pp. 425–429, 2002.

[34] P. K. Seidelmann, *Explanatory Supplement to the Astronomical Almanac*. University Science Books, 2005, p. 36.

[35] Solvay, “Typical Properties Solef Hyla.” [Online]. Available: http://www.solvayplastics.com/sites/solvayplastics/EN/Solvay Plastics Literature/Typical_Properties_Solef_Hylar_EN.pdf. [Accessed: 30-Oct-2012].
[36] Sigma-Aldrich, “Hexane Physical Properties Chart.” [Online]. Available: https://www.sigmaaldrich.com/chemistry/solvents/hexane-center/physical-properties.html. [Accessed: 20-Jun-2012].

SUMMARY IN ESTONIAN

Polüvinüleendifluoriidi kasutamine “twisting-ball” tüüpi kuvari aktiivelemendi valmistamiseks

Töö eesmärgiks oli näidata PVDF (polüvinüleendifluoriid) kasutamise võimalikkust *twisting-ball* tüüpi kuvari aktiivelemendi valmistamiseks.

Twisting-ball on e-paberi tüüp, milles kujutise moodustavad kahevärvilised polariseeritud pallikesed, mis on paigutatud läbipaistvasse kilesse ja mis muudavad oma orientatsiooni välise juhtpinge muutumisel. Sellisekuvari leiutas Nicholas Sheridon Xeroxi Palo Alto uurimiskeskuses eelmise sajandi seitsmekümnendatel. Aktiivelemendi valmistamiseks kasutati vahasid ja hiljem polüetüleeni. Pallide polariseerimine toimus erineva laenguga sulatatud materjalitilgakeste liitmisega, mis tingis ebaühtlase laengu. Samuti oli dipoolne laeng ebapiisav, mistõttu oli vaja kasutada väga kõrgeid juhtpingeid (raske saavutada portatiivsetes seadmetes). Nii lõpetas Xerox seda tüüpi kuvari arendamise.

PVDF on üks tugevamaid ja stabiilsemaid elektreete tänu sellele, et polariseerimisel toimub kristallstruktuuri muutumine ja polariseeritud kristalli (β-faas) siseenergia on madalam polariseerimata kristalli omast (α-faas). Tema rakendamise teeb raskeks äärmine hüdrofoobsus. See välistab osakeste värvimise, katmise jms.

Käesolevas uurimuses leiti meetod PVDF pinna funktsionaliseerimiseks. Selleks kasvatati PVDF molekulide külge ATRP reaktsiooni kasutades polüstüreeni ahelad. Suhteliselt hüdrofiilses polüstüreenikihis tekitati seejärel alumiiniumhüdroksiidi kristallisatsioonitsentrid. Neist lähtudes sadestati pinnale sol-gel meetodil suhteliselt paks (2 μm) bohemiidikiht, mis tagas osakeste valge värvuse, läbipaistmatuse ja võimaluse pinda värvida.

Töödeldud osakesed polariseeriti, värviti üks poolkera ja paigutati silikoonkilesse. Iga osakese ümber tekitati kandevedelikuga täidetud õõnsus, milles see sai vabalt pöörelda. Saadud kile paigutati kahe elektroodi vahele (vaatajapoolne elektrood läbipaistev) ja uuriti kuvari käitumist.

Töötati välja osakese käitumist kirjeldav matemaatiline mudel (diferentsiaalvõrrandite süsteem), mis lahendati Runge-Kutta meetodil, kasutades programmi MATHLAB.

Tulemusena tõestati uuritava materjali sobivus antud tüüpi kuvari valmistamiseks ja töötati välja tehnoloogiline järjestus.

ACKNOWLEDGEMENTS

The present study was performed at the Institute of Chemistry of the University of Tartu. I am very thankful to Prof Jaak Järv and Prof Toomas Tenno, my research supervisors.

I wish to thank my coauthors Dr Ivar Zekker, Dr Dmitri Panov, Dr Väino Sammelselg and Dr Peep Miidla from Tartu University.

Special thanks go to Dr Bernard Goffaux from Solvay Solexis for providing the raw materials and to Prof Urve Kallavus from Tallinn Technical University for providing access to the analytical equipment used.

PUBLICATIONS

CURRICULUM VITAE

Name:	Jüri Liiv
Date of birth:	December 24th, 1964
Citizenship:	Estonia
Address:	Kullava 1–2/4, Kolga, Kuusalu vald, 74602 Harjumaa
Phone:	+372 528 3238
E-mail:	jyriliiv@gmail.com

Education

2009–2014	Tartu University, PhD student
1981–1987	Tallinn University of Technology, electronics and semiconductor technology, MEng 1987
1978–1981	Gustav Adolfi Gümnaasium (Tallinn Secondary School No. 1)

Career

2007–2012	Visitret Displays Plc, CTO
2003–2005	TII Systems, Manager
2001–2003	Valvesilm, Project Manager
1999–2001	Informatics Centre / State Chancellery, National program "KülaTee", Program Coordinator
1996–1997	BNS, Editor
1994–1996	Estonian Business School, Associate Professor
1989–1993	Sarved ja Sõrad, Manager, Member of the board
1988–1989	Cross Development, Export-import manager
1987–1988	ELKE International, Director
1986–1987	Tallinn Power Network, IT Centre, Director

ELULOOKIRJELDUS

Nimi:	Jüri Liiv
Sünniaeg:	24.12.1964
Kodakondsus:	Eesti
Aadress:	Kullava 1–2/4, Kolga, Kuusalu vald, 74602 Harjumaa
Telefon:	+372 528 3238
E-post:	jyriliiv@gmail.com

Haridus

2009–2014	Tartu Ülikool, doktorant
1981–1987	Tallinna Tehnikaülikool, tööstuselektroonika (pooljuhtide tehnoloogia), MEng
1978–1981	Gustav Adolfi Gümnaasium (Tallinna 1. Keskkool)

Teenistuskäik

2007–2012	Visitret Displays Plc, tehnoloogiadirektor
2003–2005	TII Systems, arendusjuht
2001–2003	Valvesilm, projektijuht
1999–2001	Eesti Informaatikakeskus / Riigikantselei, “KülaTee” programmijuht
1996–1997	BNS, toimetaja
1994–1996	Estonian Business School, õppejõud
1989–1993	Sarved ja Sõrad, tegevjuht
1988–1989	Cross Development, väliskaubanduse juht
1987–1988	ELKE International, director
1986–1987	Tallinn Power Network, IT Centre, director

DISSERTATIONES CHIMICAE UNIVERSITATIS TARTUENSIS

1. **Toomas Tamm.** Quantum-chemical simulation of solvent effects. Tartu, 1993, 110 p.
2. **Peeter Burk.** Theoretical study of gas-phase acid-base equilibria. Tartu, 1994, 96 p.
3. **Victor Lobanov.** Quantitative structure-property relationships in large descriptor spaces. Tartu, 1995, 135 p.
4. **Vahur Mäemets.** The ^{17}O and ^{1}H nuclear magnetic resonance study of H_2O in individual solvents and its charged clusters in aqueous solutions of electrolytes. Tartu, 1997, 140 p.
5. **Andrus Metsala.** Microcanonical rate constant in nonequilibrium distribution of vibrational energy and in restricted intramolecular vibrational energy redistribution on the basis of slater's theory of unimolecular reactions. Tartu, 1997, 150 p.
6. **Uko Maran.** Quantum-mechanical study of potential energy surfaces in different environments. Tartu, 1997, 137 p.
7. **Alar Jänes.** Adsorption of organic compounds on antimony, bismuth and cadmium electrodes. Tartu, 1998, 219 p.
8. **Kaido Tammeveski.** Oxygen electroreduction on thin platinum films and the electrochemical detection of superoxide anion. Tartu, 1998, 139 p.
9. **Ivo Leito.** Studies of Brønsted acid-base equilibria in water and non-aqueous media. Tartu, 1998, 101 p.
10. **Jaan Leis.** Conformational dynamics and equilibria in amides. Tartu, 1998, 131 p.
11. **Toonika Rinken.** The modelling of amperometric biosensors based on oxidoreductases. Tartu, 2000, 108 p.
12. **Dmitri Panov.** Partially solvated Grignard reagents. Tartu, 2000, 64 p.
13. **Kaja Orupõld.** Treatment and analysis of phenolic wastewater with microorganisms. Tartu, 2000, 123 p.
14. **Jüri Ivask.** Ion Chromatographic determination of major anions and cations in polar ice core. Tartu, 2000, 85 p.
15. **Lauri Vares.** Stereoselective Synthesis of Tetrahydrofuran and Tetrahydropyran Derivatives by Use of Asymmetric Horner-Wadsworth-Emmons and Ring Closure Reactions. Tartu, 2000, 184 p.
16. **Martin Lepiku.** Kinetic aspects of dopamine D_2 receptor interactions with specific ligands. Tartu, 2000, 81 p.
17. **Katrin Sak.** Some aspects of ligand specificity of P2Y receptors. Tartu, 2000, 106 p.
18. **Vello Pällin.** The role of solvation in the formation of iotsitch complexes. Tartu, 2001, 95 p.

19. **Katrin Kollist.** Interactions between polycyclic aromatic compounds and humic substances. Tartu, 2001, 93 p.
20. **Ivar Koppel.** Quantum chemical study of acidity of strong and superstrong Brønsted acids. Tartu, 2001, 104 p.
21. **Viljar Pihl.** The study of the substituent and solvent effects on the acidity of OH and CH acids. Tartu, 2001, 132 p.
22. **Natalia Palm.** Specification of the minimum, sufficient and significant set of descriptors for general description of solvent effects. Tartu, 2001, 134 p.
23. **Sulev Sild.** QSPR/QSAR approaches for complex molecular systems. Tartu, 2001, 134 p.
24. **Ruslan Petrukhin.** Industrial applications of the quantitative structure-property relationships. Tartu, 2001, 162 p.
25. **Boris V. Rogovoy.** Synthesis of (benzotriazolyl)carboximidamides and their application in relations with *N*- and *S*-nucleophyles. Tartu, 2002, 84 p.
26. **Koit Herodes.** Solvent effects on UV-vis absorption spectra of some solvatochromic substances in binary solvent mixtures: the preferential solvation model. Tartu, 2002, 102 p.
27. **Anti Perkson.** Synthesis and characterisation of nanostructured carbon. Tartu, 2002, 152 p.
28. **Ivari Kaljurand.** Self-consistent acidity scales of neutral and cationic Brønsted acids in acetonitrile and tetrahydrofuran. Tartu, 2003, 108 p.
29. **Karmen Lust.** Adsorption of anions on bismuth single crystal electrodes. Tartu, 2003, 128 p.
30. **Mare Piirsalu.** Substituent, temperature and solvent effects on the alkaline hydrolysis of substituted phenyl and alkyl esters of benzoic acid. Tartu, 2003, 156 p.
31. **Meeri Sassian.** Reactions of partially solvated Grignard reagents. Tartu, 2003, 78 p.
32. **Tarmo Tamm.** Quantum chemical modelling of polypyrrole. Tartu, 2003. 100 p.
33. **Erik Teinemaa.** The environmental fate of the particulate matter and organic pollutants from an oil shale power plant. Tartu, 2003. 102 p.
34. **Jaana Tammiku-Taul.** Quantum chemical study of the properties of Grignard reagents. Tartu, 2003. 120 p.
35. **Andre Lomaka.** Biomedical applications of predictive computational chemistry. Tartu, 2003. 132 p.
36. **Kostyantyn Kirichenko.** Benzotriazole – Mediated Carbon–Carbon Bond Formation. Tartu, 2003. 132 p.
37. **Gunnar Nurk.** Adsorption kinetics of some organic compounds on bismuth single crystal electrodes. Tartu, 2003, 170 p.
38. **Mati Arulepp.** Electrochemical characteristics of porous carbon materials and electrical double layer capacitors. Tartu, 2003, 196 p.

39. **Dan Cornel Fara.** QSPR modeling of complexation and distribution of organic compounds. Tartu, 2004, 126 p.
40. **Riina Mahlapuu.** Signalling of galanin and amyloid precursor protein through adenylate cyclase. Tartu, 2004, 124 p.
41. **Mihkel Kerikmäe.** Some luminescent materials for dosimetric applications and physical research. Tartu, 2004, 143 p.
42. **Jaanus Kruusma.** Determination of some important trace metal ions in human blood. Tartu, 2004, 115 p.
43. **Urmas Johanson.** Investigations of the electrochemical properties of polypyrrole modified electrodes. Tartu, 2004, 91 p.
44. **Kaido Sillar.** Computational study of the acid sites in zeolite ZSM-5. Tartu, 2004, 80 p.
45. **Aldo Oras.** Kinetic aspects of dATPαS interaction with $P2Y_1$ receptor. Tartu, 2004, 75 p.
46. **Erik Mölder.** Measurement of the oxygen mass transfer through the air-water interface. Tartu, 2005, 73 p.
47. **Thomas Thomberg.** The kinetics of electroreduction of peroxodisulfate anion on cadmium (0001) single crystal electrode. Tartu, 2005, 95 p.
48. **Olavi Loog.** Aspects of condensations of carbonyl compounds and their imine analogues. Tartu, 2005, 83 p.
49. **Siim Salmar.** Effect of ultrasound on ester hydrolysis in aqueous ethanol. Tartu, 2006, 73 p.
50. **Ain Uustare.** Modulation of signal transduction of heptahelical receptors by other receptors and G proteins. Tartu, 2006, 121 p.
51. **Sergei Yurchenko.** Determination of some carcinogenic contaminants in food. Tartu, 2006, 143 p.
52. **Kaido Tämm.** QSPR modeling of some properties of organic compounds. Tartu, 2006, 67 p.
53. **Olga Tšubrik.** New methods in the synthesis of multisubstituted hydrazines. Tartu. 2006, 183 p.
54. **Lilli Sooväli.** Spectrophotometric measurements and their uncertainty in chemical analysis and dissociation constant measurements. Tartu, 2006, 125 p.
55. **Eve Koort.** Uncertainty estimation of potentiometrically measured ph and pK_a values. Tartu, 2006, 139 p.
56. **Sergei Kopanchuk.** Regulation of ligand binding to melanocortin receptor subtypes. Tartu, 2006, 119 p.
57. **Silvar Kallip.** Surface structure of some bismuth and antimony single crystal electrodes. Tartu, 2006, 107 p.
58. **Kristjan Saal.** Surface silanization and its application in biomolecule coupling. Tartu, 2006, 77 p.
59. **Tanel Tätte.** High viscosity $Sn(OBu)_4$ oligomeric concentrates and their applications in technology. Tartu, 2006, 91 p.

60. **Dimitar Atanasov Dobchev**. Robust QSAR methods for the prediction of properties from molecular structure. Tartu, 2006, 118 p.
61. **Hannes Hagu**. Impact of ultrasound on hydrophobic interactions in solutions. Tartu, 2007, 81 p.
62. **Rutha Jäger.** Electroreduction of peroxodisulfate anion on bismuth electrodes. Tartu, 2007, 142 p.
63. **Kaido Viht.** Immobilizable bisubstrate-analogue inhibitors of basophilic protein kinases: development and application in biosensors. Tartu, 2007, 88 p.
64. **Eva-Ingrid Rõõm.** Acid-base equilibria in nonpolar media. Tartu, 2007, 156 p.
65. **Sven Tamp.** DFT study of the cesium cation containing complexes relevant to the cesium cation binding by the humic acids. Tartu, 2007, 102 p.
66. **Jaak Nerut.** Electroreduction of hexacyanoferrate(III) anion on Cadmium (0001) single crystal electrode. Tartu, 2007, 180 p.
67. **Lauri Jalukse.** Measurement uncertainty estimation in amperometric dissolved oxygen concentration measurement. Tartu, 2007, 112 p.
68. **Aime Lust.** Charge state of dopants and ordered clusters formation in CaF_2:Mn and CaF_2:Eu luminophors. Tartu, 2007, 100 p.
69. **Iiris Kahn**. Quantitative Structure-Activity Relationships of environmentally relevant properties. Tartu, 2007, 98 p.
70. **Mari Reinik.** Nitrates, nitrites, N-nitrosamines and polycyclic aromatic hydrocarbons in food: analytical methods, occurrence and dietary intake. Tartu, 2007, 172 p.
71. **Heili Kasuk.** Thermodynamic parameters and adsorption kinetics of organic compounds forming the compact adsorption layer at Bi single crystal electrodes. Tartu, 2007, 212 p.
72. **Erki Enkvist.** Synthesis of adenosine-peptide conjugates for biological applications. Tartu, 2007, 114 p.
73. **Svetoslav Hristov Slavov**. Biomedical applications of the QSAR approach. Tartu, 2007, 146 p.
74. **Eneli Härk.** Electroreduction of complex cations on electrochemically polished Bi(*hkl*) single crystal electrodes. Tartu, 2008, 158 p.
75. **Priit Möller.** Electrochemical characteristics of some cathodes for medium temperature solid oxide fuel cells, synthesized by solid state reaction technique. Tartu, 2008, 90 p.
76. **Signe Viggor.** Impact of biochemical parameters of genetically different pseudomonads at the degradation of phenolic compounds. Tartu, 2008, 122 p.
77. **Ave Sarapuu.** Electrochemical reduction of oxygen on quinone-modified carbon electrodes and on thin films of platinum and gold. Tartu, 2008, 134 p.
78. **Agnes Kütt.** Studies of acid-base equilibria in non-aqueous media. Tartu, 2008, 198 p.

79. **Rouvim Kadis.** Evaluation of measurement uncertainty in analytical chemistry: related concepts and some points of misinterpretation. Tartu, 2008, 118 p.
80. **Valter Reedo.** Elaboration of IVB group metal oxide structures and their possible applications. Tartu, 2008, 98 p.
81. **Aleksei Kuznetsov.** Allosteric effects in reactions catalyzed by the cAMP-dependent protein kinase catalytic subunit. Tartu, 2009, 133 p.
82. **Aleksei Bredihhin.** Use of mono- and polyanions in the synthesis of multisubstituted hydrazine derivatives. Tartu, 2009, 105 p.
83. **Anu Ploom.** Quantitative structure-reactivity analysis in organosilicon chemistry. Tartu, 2009, 99 p.
84. **Argo Vonk.** Determination of adenosine A_{2A}- and dopamine D_1 receptor-specific modulation of adenylate cyclase activity in rat striatum. Tartu, 2009, 129 p.
85. **Indrek Kivi.** Synthesis and electrochemical characterization of porous cathode materials for intermediate temperature solid oxide fuel cells. Tartu, 2009, 177 p.
86. **Jaanus Eskusson.** Synthesis and characterisation of diamond-like carbon thin films prepared by pulsed laser deposition method. Tartu, 2009, 117 p.
87. **Marko Lätt.** Carbide derived microporous carbon and electrical double layer capacitors. Tartu, 2009, 107 p.
88. **Vladimir Stepanov.** Slow conformational changes in dopamine transporter interaction with its ligands. Tartu, 2009, 103 p.
89. **Aleksander Trummal.** Computational Study of Structural and Solvent Effects on Acidities of Some Brønsted Acids. Tartu, 2009, 103 p.
90. **Eerold Vellemäe.** Applications of mischmetal in organic synthesis. Tartu, 2009, 93 p.
91. **Sven Parkel.** Ligand binding to 5-HT_{1A} receptors and its regulation by Mg^{2+} and Mn^{2+}. Tartu, 2010, 99 p.
92. **Signe Vahur.** Expanding the possibilities of ATR-FT-IR spectroscopy in determination of inorganic pigments. Tartu, 2010, 184 p.
93. **Tavo Romann**. Preparation and surface modification of bismuth thin film, porous, and microelectrodes. Tartu, 2010, 155 p.
94. **Nadežda Aleksejeva.** Electrocatalytic reduction of oxygen on carbon nanotube-based nanocomposite materials. Tartu, 2010, 147 p.
95. **Marko Kullapere.** Electrochemical properties of glassy carbon, nickel and gold electrodes modified with aryl groups. Tartu, 2010, 233 p.
96. **Liis Siinor.** Adsorption kinetics of ions at Bi single crystal planes from aqueous electrolyte solutions and room-temperature ionic liquids. Tartu, 2010, 101 p.
97. **Angela Vaasa.** Development of fluorescence-based kinetic and binding assays for characterization of protein kinases and their inhibitors. Tartu 2010, 101 p.

98. **Indrek Tulp.** Multivariate analysis of chemical and biological properties. Tartu 2010, 105 p.
99. **Aare Selberg.** Evaluation of environmental quality in Northern Estonia by the analysis of leachate. Tartu 2010, 117 p.
100. **Darja Lavõgina.** Development of protein kinase inhibitors based on adenosine analogue-oligoarginine conjugates. Tartu 2010, 248 p.
101. **Laura Herm.** Biochemistry of dopamine D_2 receptors and its association with motivated behaviour. Tartu 2010, 156 p.
102. **Terje Raudsepp.** Influence of dopant anions on the electrochemical properties of polypyrrole films. Tartu 2010, 112 p.
103. **Margus Marandi.** Electroformation of Polypyrrole Films: *In-situ* AFM and STM Study. Tartu 2011, 116 p.
104. **Kairi Kivirand.** Diamine oxidase-based biosensors: construction and working principles. Tartu, 2011, 140 p.
105. **Anneli Kruve.** Matrix effects in liquid-chromatography electrospray mass-spectrometry. Tartu, 2011, 156 p.
106. **Gary Urb.** Assessment of environmental impact of oil shale fly ash from PF and CFB combustion. Tartu, 2011, 108 p.
107. **Nikita Oskolkov.** A novel strategy for peptide-mediated cellular delivery and induction of endosomal escape. Tartu, 2011, 106 p.
108. **Dana Martin.** The QSPR/QSAR approach for the prediction of properties of fullerene derivatives. Tartu, 2011, 98 p.
109. **Säde Viirlaid.** Novel glutathione analogues and their antioxidant activity. Tartu, 2011, 106 p.
110. **Ülis Sõukand.** Simultaneous adsorption of Cd^{2+}, Ni^{2+}, and Pb^{2+} on peat. Tartu, 2011, 124 p.
111. **Lauri Lipping.** The acidity of strong and superstrong Brønsted acids, an outreach for the "limits of growth": a quantum chemical study. Tartu, 2011, 124 p.
112. **Heisi Kurig.** Electrical double-layer capacitors based on ionic liquids as electrolytes. Tartu, 2011, 146 p.
113. **Marje Kasari.** Bisubstrate luminescent probes, optical sensors and affinity adsorbents for measurement of active protein kinases in biological samples. Tartu, 2012, 126 p.
114. **Kalev Takkis.** Virtual screening of chemical databases for bioactive molecules. Tartu, 2012, 122 p.
115. **Ksenija Kisseljova**. Synthesis of aza-β^3-amino acid containing peptides and kinetic study of their phosphorylation by protein kinase A. Tartu, 2012, 104 p.
116. **Riin Rebane.** Advanced method development strategy for derivatization LC/ESI/MS. Tartu, 2012, 184 p.

117. **Vladislav Ivaništšev.** Double layer structure and adsorption kinetics of ions at metal electrodes in room temperature ionic liquids. Tartu, 2012, 128 p.
118. **Irja Helm.** High accuracy gravimetric Winkler method for determination of dissolved oxygen. Tartu, 2012, 139 p.
119. **Karin Kipper.** Fluoroalcohols as Components of LC-ESI-MS Eluents: Usage and Applications. Tartu, 2012, 164 p.
120. **Arno Ratas.** Energy storage and transfer in dosimetric luminescent materials. Tartu, 2012, 163 p.
121. **Reet Reinart-Okugbeni**. Assay systems for characterisation of subtype-selective binding and functional activity of ligands on dopamine receptors. Tartu, 2012, 159 p.
122. **Lauri Sikk.** Computational study of the Sonogashira cross-coupling reaction. Tartu, 2012, 81 p.
123. **Karita Raudkivi.** Neurochemical studies on inter-individual differences in affect-related behaviour of the laboratory rat. Tartu, 2012, 161 p.
124. **Indrek Saar.** Design of GalR2 subtype specific ligands: their role in depression-like behavior and feeding regulation. Tartu, 2013, 126 p.
125. **Ann Laheäär.** Electrochemical characterization of alkali metal salt based non-aqueous electrolytes for supercapacitors. Tartu, 2013, 127 p.
126. **Kerli Tõnurist.** Influence of electrospun separator materials properties on electrochemical performance of electrical double-layer capacitors. Tartu, 2013, 147 p.
127. **Kaija Põhako-Esko.** Novel organic and inorganic ionogels: preparation and characterization. Tartu, 2013, 124 p.
128. **Ivar Kruusenberg.** Electroreduction of oxygen on carbon nanomaterial-based catalysts. Tartu, 2013, 191 p.
129. **Sander Piiskop.** Kinetic effects of ultrasound in aqueous acetonitrile solutions. Tartu, 2013, 95 p.
130. **Ilona Faustova**. Regulatory role of L-type pyruvate kinase N-terminal domain. Tartu, 2013, 109 p.
131. **Kadi Tamm.** Synthesis and characterization of the micro-mesoporous anode materials and testing of the medium temperature solid oxide fuel cell single cells. Tartu, 2013, 138 p.
132. **Iva Bozhidarova Stoyanova-Slavova.** Validation of QSAR/QSPR for regulatory purposes. Tartu, 2013, 109 p.
133. **Vitali Grozovski**. Adsorption of organic molecules at single crystal electrodes studied by *in situ* STM method. Tartu, 2014, 146 p.
134. **Santa Veikšina**. Development of assay systems for characterisation of ligand binding properties to melanocortin 4 receptors. Tartu, 2014, 151 p.